Dynamical evolution of boson stars. II. Excited states and self-interacting fields

Jayashree Balakrishna
McDonnell Center for the Space Sciences, Washington University, St. Louis, Missouri 63130

Edward Seidel
National Center for Supercomputing Applications, University of Illinois, Champaign, Illinois 61820
and Departments of Physics and Astronomy, University of Illinois, Champaign, Illinois 61820
and Max-Planck-Institut für Gravitationsphysik, 14473 Potsdam, Germany

Wai-Mo Suen
McDonnell Center for the Space Sciences, Washington University, St. Louis, Missouri 63130
and Physics Department, Chinese University of Hong Kong, Hong Kong, China
(Received 15 December 1997; published 30 September 1998)

The dynamical evolution of self-gravitating scalar field configurations in numerical relativity is studied. The previous analysis on ground state boson stars of non-interacting fields is extended to excited states and to fields with self-couplings. Self-couplings can significantly change the physical dimensions of boson stars, making them much more astrophysically interesting (e.g., having mass of the order of 0.1 solar mass). The stable (S) and unstable (U) branches of equilibrium configurations of boson stars of self-interacting fields are studied; their behavior under perturbations and their quasi-normal oscillation frequencies are determined and compared to the non-interacting case. Excited states of boson stars with and without self-couplings are studied and compared. Excited states also have equilibrium configurations with S and U branch structures; both branches are intrinsically unstable under a generic perturbation but have very different instability time scales. We carry out a detailed study of the instability time scales of these configurations. It is found that highly excited states spontaneously decay through a cascade of intermediate states similar to atomic transitions.
[S0556-2821(98)02220-6]

PACS number(s): 04.40.Dg

I. INTRODUCTION

Various particle physics models suggest that bosons might play an important role in the evolution of the universe. These models predict the abundant production of these bosonic particles in the early universe and their presence in large numbers even today. Although the bosonic particles have never actually been directly detected, they are considered as leading candidates of dark matter [1]. These bosons could by a Jeans instability mechanism [2] condense into compact gravitating objects such as boson stars.

Boson stars are made up of self-gravitating complex scalar fields with or without further self-coupling [3,4]. The equilibrium configurations represent an exact balance between the attractive effect of gravity and the natural tendency for the scalar field to disperse. The stability of such an object is hence a central issue. It is well known that equilibrium configurations of boson stars have stable (S) and unstable (U) branches as well as a hierarchy of ground and excited states [3–13]. Recently a review paper has also appeared in addition to those in [3] and [4] which outlines all the relevant boson star literature [14]. In the first paper in this series [5], the dynamical evolution under various perturbations of ground state boson stars made up of non-self-interacting scalar fields was studied.

In the absence of self-coupling the mass profile of the ground state configurations, when plotted against the central density $\phi(0)$, has a peak at $M=0.633m_{Pl}^2/m$ (where m_{Pl} refers to the Planck mass) corresponding to a mass of about 10^{11} kg at $\phi(0)_c=0.271$ (for bosons of mass $m=1$ GeV). Configurations for which $\phi(0)<\phi(0)_c$ (the S branch) are stable to perturbations [5,12] while those with $\phi(0)>\phi(0)_c$ (the U branch) are unstable. Stability here refers to the ability of a $\phi(0)<\phi(0)_c$ star to settle to a new configuration in the same branch under perturbations. A $\phi(0)>\phi(0)_c$ configuration star is unstable in that, upon perturbations, it cannot stay on the same branch. If it cannot lose enough mass and settle to a stable state, it either collapses to a black hole or disperses to infinity. Stable boson stars have very specific quasinormal modes of oscillation under perturbations, a feature important for the detection and identification of these stars.

In the present paper the study of paper I [5] is extended to the excited state boson star and to the case of a $\lambda\phi^4$ self-interacting scalar field. The dynamical evolutions of such systems are studied numerically.

The action for the system studied in this paper is given by

$$I=\frac{1}{16\pi G}\int d^4x\sqrt{-g}R-\int d^4x\left[\sqrt{-g}\left(\frac{1}{2}g^{\mu\nu}\partial_\mu\Phi^*\partial_\nu\Phi+\frac{1}{2}m^2\Phi^*\Phi+\frac{1}{4}\lambda|\Phi|^4\right)\right]. \tag{1.1}$$

There are two reasons to include the self-coupling interaction [6,8]. First, without the $\lambda\phi^4$ term, the maximum mass of a boson star,

$$M = 0.633 m_{Pl}^2/m \tag{1.2}$$

(where m_{Pl} refers to the Planck mass and m the mass of the boson), could be too small to be astrophysically significant. For example, for $m=1$ GeV, $M=10^{-19}M_\odot$ where $M_\odot$ is the solar mass. On the other hand, for interacting fields, even with a small coupling, the mass of the star can be large [6]. In this case,

$$M \sim 0.06\sqrt{\lambda}\,\frac{m_{Pl}^3}{m^2}, \tag{1.3}$$

which is larger than Eq. (1.2) by a factor of $\sim\sqrt{\lambda}m_{Pl}/m \sim 10^{19}\sqrt{\lambda}$, for $m=1$ GeV. A moderate value of $\lambda=0.01$ then leads to $M=0.1M_\odot$, which is particularly interesting due to the gravitational microlensing data [15]. (It should be noted, however, that for smaller values of bosonic mass m one can have boson stars of the order of solar masses even without self-coupling [16]).

Second, boson stars give us a way to study local anisotropy and its effects. The larger the self-coupling parameter λ, the smaller the fractional anisotropy. Changing the self-coupling parameter for a given central density provides a way to vary this anisotropy in a natural way [8]. By anisotropy we mean that the radial and tangential components of the pressure are different. This is of interest because deviations from perfect fluid assumptions for even nuclear matter is expected in the presence of strong gravitational fields. In boson stars this anisotropy appears very naturally. Although we have not studied specifically the anisotropies in this paper, it provides motivation for adding a self-coupling term.

The results of paper I are also extended by considering the evolution of excited states with and without self-coupling. This is of importance because if boson stars exist and are detected, they are most likely those interacting with their environment and going through some excitation process. Excited configurations might also be intermediate stages during the formation process of these stars. In this study the configurations considered are spherically symmetric; all perturbations of equilibrium configurations are purely radial. Full 3D simulations are underway and will be reported in a future paper. The remainder of this paper is organized as follows:

Section II sets up the mathematical foundations of the problem, including the equilibrium and evolution equations. The calculation of the initial data sets is discussed and the techniques used to evolve the system numerically are briefly outlined.

Section III details the evolution of ground state configurations with self-coupling. We show that they have similar *S* and *U* branch structures as boson stars without self-coupling. *S* branch stars are stable with regard to perturbations. By this we mean that under small perturbations they return to configurations on the same branch although not to the same configurations. We studied in detail the fundamental quasinormal modes of oscillation of *S*-branch stars [those for which $\phi(0)<\phi(0)_c$]. They are important characteristics for observations. They can also be used to predict the end point of the evolution of perturbed stars, as well as a comparison between modes for different self-couplings. In the next subsection of Sec. III, the migration of a *U*-branch star [that for which $\phi(0)>\phi(0)_c$] to the *S*-branch is described. The essential features of the $\lambda=0$ case are retained. If a *U*-branch star is perturbed by the addition of mass, the star will collapse to a black hole. When, as a result of perturbation, the star's mass is reduced, corresponding to annihilation of scalar particles, the star expands and moves to the *S*-branch, oscillates, and settles to a new equilibrium configuration of lower mass.

Section IV studies various aspects of the evolution of excited states. Excited states have similar band structures to ground state stars. In this paper, we study generic perturbations that may exist for a boson star in an astrophysical environment, e.g., some additional scalar particles falling in. The *S*-branch excited states have previously been found to be stable under infinitesimal perturbations that conserve the total mass and particle number of the boson star [4]. We find that these stars are inherently unstable irrespective of whether they lie on the *S* or the *U* branch but the time scales of instability are different. This result is consistent with the study of infinitesimal perturbations [12]. If they cannot lose enough mass to transit to the ground state, they either collapse to black holes or, as in the case of stars for which $M>Nm$ ($M=$mass of the star, $N=$number of bosons and $m=$mass of one boson), disperse to infinity. The decay of some higher excited configurations is also studied. These higher node configurations cascade through intermediate configurations of lower excited states on their way to collapse. This is reminiscent of atomic transitions where atoms go from an excited state to lower states through intermediate ones, lending credence to the idea that boson stars are like gravitational atoms [3]. A brief conclusion follows in Sec. V. An appendix at the end shows some features of the the high Λ ($\Lambda=\lambda/4\pi m^2 G$) configurations, including a calculation of quasinormal modes.

II. FORMULATION AND EQUILIBRIUM MODELS

In this section the mathematical formulation of the problem, the creation of the equilibrium and perturbed boson star modes and the numerical code used to study them are described. The formulation is the same as that of paper I in this series [5] except for the self-interaction term. The numerical treatment used in this code has various improvements over that described in paper I. Some details of the numerical code, e.g., convergence tests etc., which are similar to those reported in paper I will not be repeated here.

The action for a self-gravitating scalar field given by Eq. (1.1) leads to the scalar field equation

$$g^{\mu\nu}\Phi_{;\mu\nu} - m^2\Phi - \lambda(\Phi^*\Phi)\Phi = 0 \tag{2.1}$$

for the complex scalar field $\Phi=\Phi_1+i\Phi_2$ and the Einstein field equations

$$R_{\mu\nu} - \frac{1}{2}g_{\mu\nu}R = 8\pi G T_{\mu\nu}.$$

The metric for this spherically symmetric system can be written as

$$ds^2 = -\mathbf{N}^2 d\mathbf{t}^2 + \mathbf{g}^2 d\mathbf{r}^2 + \mathbf{r}^2 d\mathbf{\Omega}^2, \tag{2.2}$$

where **g**, the radial metric, and **N**, the lapse, are functions of (**t**,**r**) with **r** being the circumferential radius. This form of the metric is known as the radial gauge. In the absence of a shift vector β^a, this form of the metric can be maintained for all time by enforcing the polar slicing condition. This is a condition on the lapse that requires $K_{\theta\theta} + K_{\phi\phi} = 0$ where K_{ij} is the extrinsic curvature tensor. This slicing condition causes the lapse **N** to decrease rapidly if an apparent horizon is approached [17].

The equilibrium boson star configurations are those in which the metric is time independent. The scalar field Φ itself oscillates with fixed frequency ω_0:

$$\Phi(\mathbf{t},\mathbf{r}) = \Phi_0(\mathbf{r}) e^{-i\omega_0 \mathbf{t}}, \tag{2.3}$$

but due to the U(1) symmetry of the Lagrangian, the stress energy tensor and the spacetime geometry are time independent. In dimensionless coordinates we have

$$r = m\mathbf{r}, \quad t = \omega_0 \mathbf{t}, \quad \sigma = \sqrt{4\pi G}\Phi,$$
$$N = \mathbf{N}\frac{m}{\omega_0}, \quad \Lambda = \frac{\lambda}{m^2 4\pi G}, \tag{2.4}$$

and the Einstein and Klein-Gordon equations under these conditions are

$$\sigma_0' = \chi_1 \tag{2.5}$$

$$\chi_1' = -\left[\frac{1}{r} + \frac{g^2}{r} - r g^2 \sigma_0^2\right]\chi_1 - \left[\frac{1}{N^2} - 1\right]\sigma_0 g^2 + \Lambda(g^2 \sigma_0^3) \tag{2.6}$$

$$g' = \frac{1}{2}\left[\frac{g}{r} - \frac{g^3}{r} + \sigma_0^2 r g^3\left(1 + \frac{1}{N^2}\right) + r g \chi_1^2 + \frac{1}{2}\Lambda(g^3 r \sigma_0^4)\right] \tag{2.7}$$

$$N' = \frac{1}{2}\left[-\frac{N}{r} + \frac{N g^2}{r} + \frac{r g^2 \sigma_0^2}{N}(1 - N^2) + r N \chi_1^2 - \frac{1}{2}\Lambda g^2 N r \sigma_0^4\right], \tag{2.8}$$

where $\sigma_0 \equiv \Phi_0\sqrt{4\pi G}$. A prime denotes $\partial/\partial r$ and an overdot denotes $\partial/\partial t$. All quantities in this paper are reported in terms of these dimensionless parameters unless explicitly stated otherwise. Regularity at the origin requires that $g(r=0)=1$ and that all other quantities be finite at $r=0$. For the solution to represent an isolated star, it is required that $\sigma(r=\infty)=0$. This constitutes an eigenvalue problem. For each choice of $\sigma(r=0)$, the above set of equations has a solution only when $N(r=0)$ takes on certain values. Different eigenvalues correspond to a different number of nodes in the solution of $\sigma(r)$. Solutions are also obtained for different values of the coupling parameter λ. Different families of equilibrium configurations are shown in Fig. 1. The mass profile of ground state boson stars with self-coupling has the familiar structure seen in non-self-interacting fields [5] which is also found in white dwarfs and neutron stars. The mass grows to a maximum as the central density is increased, and then decreases with further increase in central density. (See Fig. 1.) The maximum mass increases with Λ but the profile is similar. The expectation, that the branch to the left of the maximum is stable (S-branch) while that to the right (U-branch) is unstable, as in the case of ground state configurations without self-coupling, is found to be true. Stability here refers to the ability of S-branch stars to settle to new S-branch configurations when perturbed, a feature of importance for the long term existence of these stars.

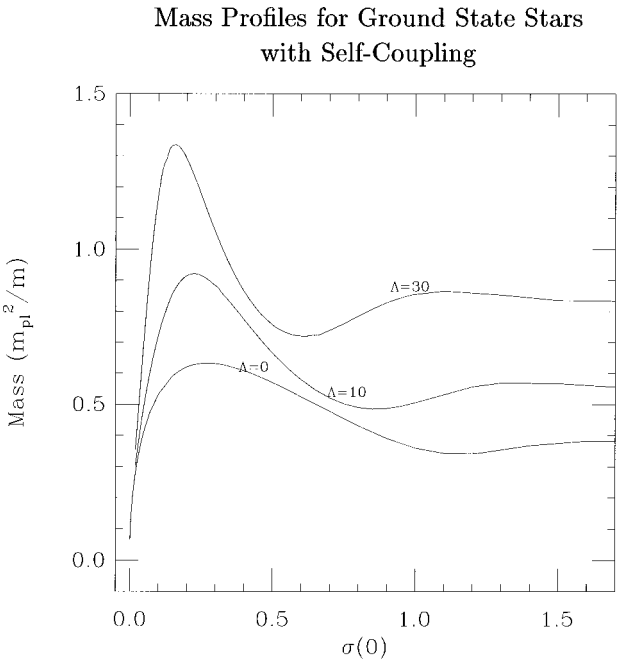

FIG. 1. The mass profiles of ground state boson stars for different values of the self-coupling constant Λ are shown. The increase in mass with Λ is clear although the profiles are very similar.

A. Evolution equations

The configurations described above are time independent, equilibrium solutions to the Einstein equations. The aim of this paper is to study their dynamical properties according to the coupled Einstein–Klein-Gordon equations. In this paper only spherically symmetric configurations are studied. In actual numerical evolution the following set of variables is chosen:

$$\psi_1 \equiv r\sigma_1, \quad \psi_2 \equiv r\sigma_2, \quad \pi_1 \equiv \frac{1}{\alpha}\frac{\partial \psi_1}{\partial t}, \quad \pi_2 \equiv \frac{1}{\alpha}\frac{\partial \psi_2}{\partial t}, \tag{2.9}$$

where

$$\alpha \equiv \frac{N}{g}, \tag{2.10}$$

and the subscripts on ψ_i denote the real and imaginary parts of the scalar field multiplied by r.

In terms of these variables and the dimensionless ones in the previous section the evolution equations are as follows: The radial metric function g evolves according to

$$\dot{g} = N(\pi_1\sigma_1' + \pi_2\sigma_2'). \tag{2.11}$$

The polar slicing equation, which is integrated on each time slice, is given by

$$N' = \frac{N}{2}\left[\frac{g^2-1}{r} + r[(\sigma_1')^2 + (\sigma_2')^2 - g^2(\sigma_1^2+\sigma_2^2)] + \frac{\pi_1^2+\pi_2^2}{r} - \frac{g^2\Lambda r}{2}(\sigma_1^2+\sigma_2^2)^2\right]. \tag{2.12}$$

The Klein-Gordon equation for the scalar field can be written as

$$\dot{\pi}_i = \alpha'\psi_i' + \alpha\psi_i'' - \psi_i\left[gN + \frac{\alpha'}{r} + \Lambda(\psi_1^2+\psi_2^2)\right], \quad i=1,2, \tag{2.13}$$

$$\dot{\psi}_i = \alpha\pi_i, \quad i=1,2. \tag{2.14}$$

The Hamiltonian constraint equation is given by

$$\frac{2g'}{rg^3} + \frac{g^2-1}{r^2g^2} - \frac{\pi_1^2+\pi_2^2}{r^2g^2} - \frac{\sigma_1'^2+\sigma_2'^2}{g^2} - (\sigma_1^2+\sigma_2^2) - \frac{\Lambda}{2}(\sigma_1^2+\sigma_2^2)^2 = 0. \tag{2.15}$$

It is not solved during the evolution, but as it is in principle conserved by the evolution equations, it is monitored closely as an indicator of the numerical accuracy of the simulation. For further details see [5].

B. Boundary conditions

Regularity conditions require that $g(r=0)=1$, and g, N, σ_1 and σ_2 have vanishing first spatial derivatives at $r=0$. To implement this condition numerically, the range of r is extended to include negative values; g, N, σ_1 and σ_2 are required to be symmetric about $r=0$. In addition ψ_1, ψ_2, π_1 and π_2 are antisymmetric about $r=0$. The antisymmetry allows the determination of ϕ_i at the origin as the first derivatives of ψ_i at $r=0$. The value of the lapse function is fixed at the outer edge on each time slice. Its value at the origin is determined by integrating Eq. (2.15) inward from the outer boundary. The value of g is determined by the evolution. The mass of the star is determined by the value of g at the edge of the grid:

$$M = \frac{1}{2}r\left[1 - \frac{1}{g^2(\infty)}\right]\frac{m_{Pl}^2}{m}, \tag{2.16}$$

where m_{Pl} is the Planck mass and m is the mass of the boson making up the star.

The boundary condition on the scalar field is an outgoing scalar wave condition. However, since the dispersion relation of the massive scalar field is non-trivial,

$$\alpha^2k^2 = \omega^2 - N^2m^2 \tag{2.17}$$

(where $\alpha = N/g$), there is no perfect algorithm for the implementation of the outgoing wave condition. Here we have adopted a two tier approach:

(i) A ''sponge'' region [5] is constructed by adding a potential term at the outer edge of the computational domain:

$$\dot{\pi}_i = \alpha'\psi_i' + \alpha\psi_i'' - \psi_i\left[gN + \frac{\alpha'}{r} + \Lambda(\psi_1^2+\psi_2^2)\right] + \frac{V}{N}(\pi_i + \psi_i'), \quad i=1,2, \quad r_N - D \leqslant r \leqslant r_N \tag{2.18}$$

where r_N is the r value of the outermost grid point and D is an adjustable parameter representing the width of the sponge. D is typically chosen to be a few times the wavelength of the scalar radiation moving out. The extra potential term in the above equation is designed to allow waves to propagate outward but damp incoming waves.

(ii) At the outermost grid point we require

$$\ddot{\psi} = -\alpha\dot{\psi}' - \frac{N^2}{2}\psi. \tag{2.19}$$

This is an exact outgoing wave condition only in the case $m=0$. The second term on the right hand side represents the finite m correction to leading order (recall that $N = \mathbf{N}m/\omega_0$). The sponge is designed to absorb the reflection coming from this approximate outgoing wave condition. We note that recent work on this problem following a hyperbolic approach seems to provide a simple and more accurate outgoing boundary condition [18].

III. DYNAMICAL EVOLUTIONS OF PERTURBED GROUND STATE STARS WITH SELF-INTERACTION

A. Nature of perturbations

We study the dynamical properties of the boson stars by perturbing the equilibrium field distribution. The accretion or annihilation of scalar particles is simulated by the addition of a field in the outer regions of the star or by decreasing it in denser regions of the star respectively. Another type of perturbation that has been effected is changing $\dot{\psi}_1$ and $\dot{\psi}_2$ of the equilibrium configuration. This perturbation changes the kinetic energy density distribution. In either case the changes in the metric functions g and N are determined by the constraint equations and the polar-slicing condition [integrating Eqs. (2.12) and (2.15) on the initial slice.] The magnitude and the length scale of the perturbations can be chosen arbitrarily. The perturbations are always spherically symmetric.

In the rest of this section we present results obtained on the dynamical evolutions of ground state equilibrium configurations perturbed in this manner. Evolutions of both

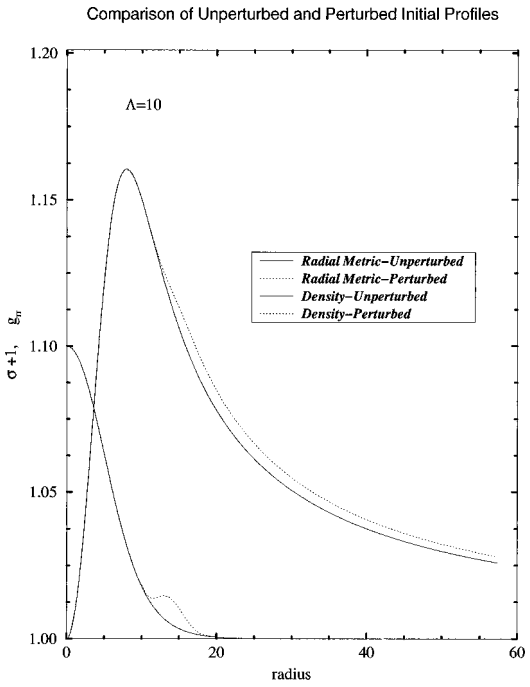

FIG. 2. The comparison of a strongly perturbed ground state $\Lambda=10$, S-branch star $[M=0.781m_{Pl}^2/m, \sigma(0)=0.1]$ to the unperturbed configuration $[M=0.722m_{Pl}^2/m]$ is shown. The solid lines correspond to the unperturbed configuration and the dashed ones to the perturbed star. The perturbation shown corresponds to the addition of a scalar-field σ at $t=0$.

S-branch and U-branch stars with and without self-coupling are considered.

B. S-branch perturbations

As shown in Ref. [5], in the free field ($\Lambda=0$) case, a perturbed S-branch star oscillates with a definite frequency, losing mass through bursts of scalar radiation at each expansion and finally settles to a new S-branch configuration of lower mass. Here the effect of a self-interacting Λ term on this behavior is examined. In Fig. 2 a typical example of the perturbed field configuration and radial metric of a star of $\Lambda=10$ with a central density of $\sigma(0)=0.1$ is shown. This star has been perturbed by accretion of scalar particles in a region of lower density. Its evolution is detailed below.

Figure 3(a) shows the radial metric as a function of distance for the same configuration at various times. The labels A,B,C,D correspond to times (in units of the inverse of the underlying scalar field frequency) $t=192,306,391,505$ respectively. The positions of the peaks are labeled R_0,R_A,R_B,R_C,R_D, where R_0 is the position of the initial unperturbed peak. Here $R_0=7.95$, $R_A=8.55$, $R_B=6.6$, $R_C=8.2$ and $R_D=6.65$ where the length scales are in terms of the inverse mass of the boson. The oscillations are shown clearly in Fig. 3(b) which is a plot of the maximum value of the radial metric as a function of time. The point where this function is a maximum corresponds to the core of the star contracting to its minimum size in a cycle. Similarly, the maximum radial metric starts to decrease as the star expands. At each expansion the star loses mass through scalar radiation. The oscillations damp out in time as the star starts settling to the new configuration. A plot of mass vs time is shown in Fig. 3(c). The amount of scalar radiation decreases in time as the oscillations damp out, as can be seen from the figure. The slope of the curve steadily decreases as the star starts settling down to its new lower mass configuration. The mass is measured at the inner edge of the sponge. Exact details of the curves have some dependence on the sponge parameters but the basic results are the same.

A characteristic of the boson star that could be important for its observation and identification is its fundamental oscillation frequency which can be determined from Fig. 3(b). We found $f=1/[199N(\infty)]=4.7\times10^{-3}$. The oscillation frequencies for a large number of S-branch stars have been compiled in this way. Figure 4(a) shows a plot of the oscillation frequency versus mass for many slightly perturbed configurations (masses within 0.1% of the unperturbed mass). As the mass increases, the frequency increases and then drops down as the transition point $[dM/d\sigma(0)=0]$ is approached, signaling the onset of instability. This is seen for both the non-self-interacting as well as the self-interacting case. These quasinormal modes of oscillation characterize S-branch stars. The point of transition from the S to the U branch corresponds to a zero frequency of oscillation [12].

Oscillations of boson stars have also been discussed using catastrophe theory in [19]. The results they find are consistent with the fundamental quasi normal-mode frequencies reported in this paper.

For a given mass higher Λ,S-branch stars have a lower oscillation frequency than similar mass lower Λ stars, unless one is near the transition point of the lower Λ configuration. This is not too surprising, since for a given mass the radius of the star increases with increasing Λ. We have seen this trend even for Λ values as high as 1600 (see discussion on high Λ stars in the Appendix). However, since the maximum mass of higher Λ configurations is greater than that of lower Λ configurations, their maximum oscillation frequency could be greater than that for lower Λ stars. (This can be understood as a size effect: on the S-branch, higher mass stars are smaller and have higher frequencies.) This can be seen in Fig. 4(a). The maximum oscillation frequencies of $\Lambda=5$ and $\Lambda=10$ configurations are higher than that of the $\Lambda=0$ case. As the stars get much larger, though, the highest frequency starts to decrease, for example the maximum frequency for $\Lambda=30$ stars being less than that of $\Lambda=15$ stars which is in itself lower than that of the $\Lambda=10$ case. A perturbation calculation for the high Λ case is shown in the Appendix to show the dependence of quasinormal mode frequencies on Λ for high Λ configurations. The frequency is proportional to the inverse of the square root of Λ. Thus as the stars get really big they oscillate less and less rapidly and numerically it is no longer feasible to evolve them. (The time step used in the numerical simulation cannot be increased as it is determined by the intrinsic oscillation time scale of the scalar field, which is many orders of magnitude shorter than the oscillation time scale of the whole star for these cases.)

The quasinormal mode curves are also useful in determining the evolutions of strongly perturbed S-branch stars and the final configurations they could settle into. A perturbed

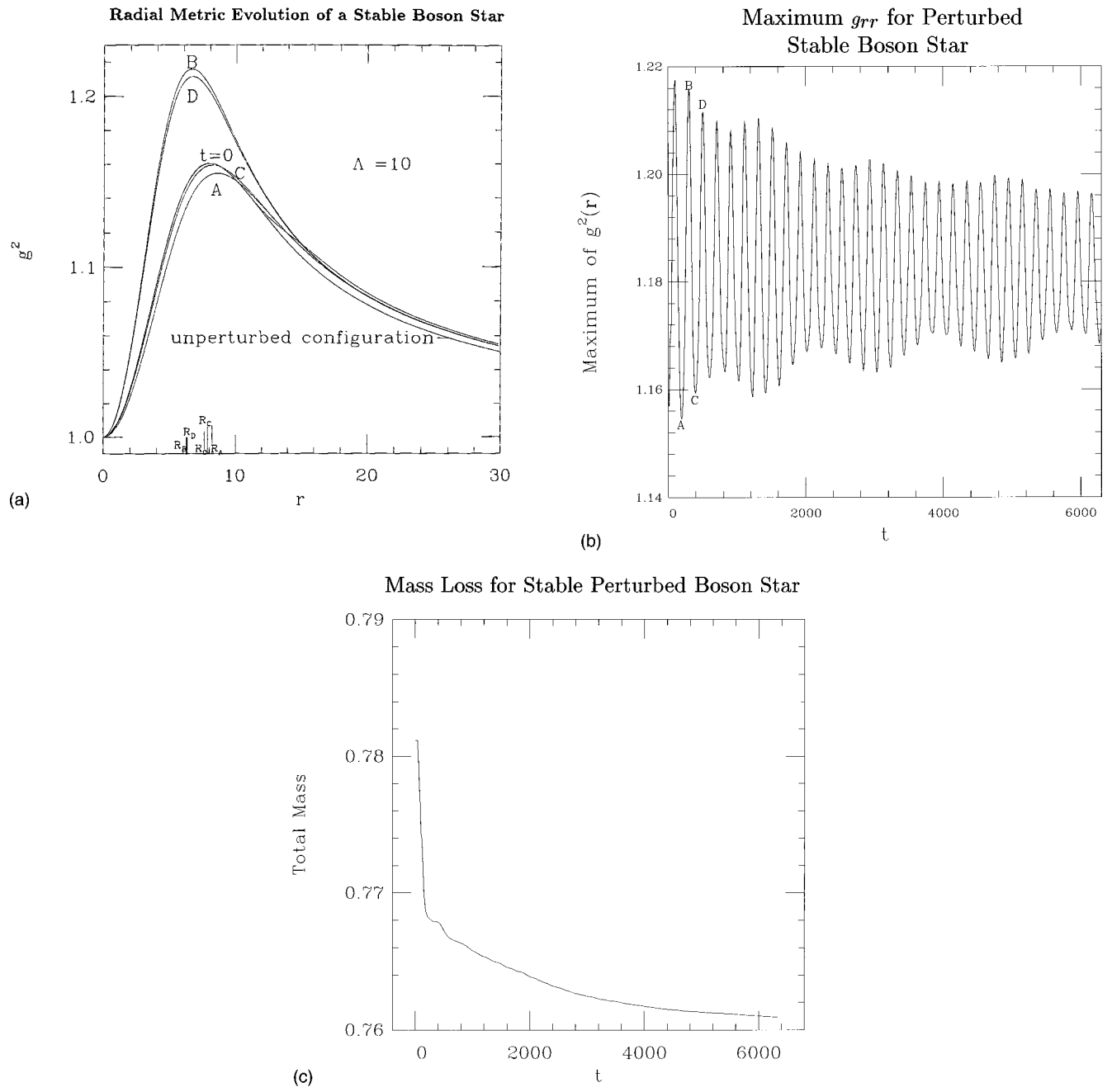

FIG. 3. (a) The evolution of the radial metric $g_{rr}=g^2$ for the configuration shown in Fig. 2. The initial perturbed configuration is labeled $t=0$. The unperturbed configuration is also shown. The spatial distributions of the radial metric labeled A,B,C,D correspond to times $t=192,306,391,505$ respectively. The radial positions of the peaks of the radial metric for these times are labeled R_A, R_B, R_C, and R_D. The values R_B and R_D are so close that they appear as one thick line in the figure. (b) The peak value of the perturbed radial metric is plotted over a long time. The points labeled A,B,C,D correspond to the same labels in (a). The oscillations decay in time. (c) The total mass of the star is plotted as a function of time. The mass loss through scalar radiation decreases in time as the oscillations start damping out.

star loses mass and settles to a final configuration corresponding to a position on the solid line in the figure. In Fig. 4(b) we single out the $\Lambda=10$ curve and plot the evolution of the S-branch star discussed above. The points $P1$, $P2$, $P3$ show the route to a new configuration. These points correspond to times $t=0$, 1200 and 4800 respectively. By extrapolating this line to where it meets the $\Lambda=10$ curve one could expect a final mass of about $.76m_{Pl}^2/m$.

C. *U*-branch perturbations

For the case of non-self-interacting fields it was shown in Ref. [5] that accretion of scalar fields causes U-branch stars to collapse to black holes. However, lowering the density can make the star migrate to the S-branch. These features are also seen in the presence of self-coupling [20]. Figure 5 shows a migrating $\Lambda=30$ star whose unperturbed overall field density σ has been decreased by about 10%. Figure 5(a)

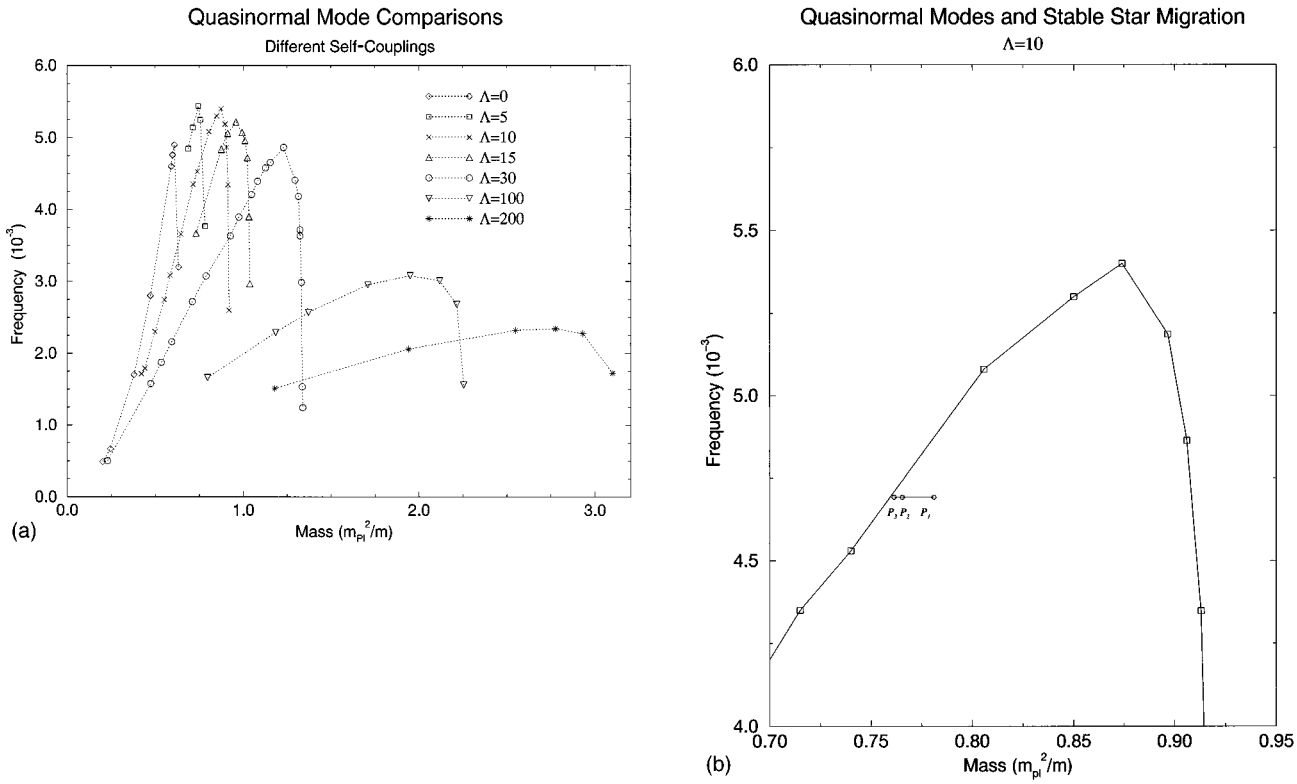

FIG. 4. (a) The oscillation frequencies of different ground state boson star configurations are plotted as functions of mass, for $\Lambda=0$, 5, 10, 15, 30, 100 and 200. The curves are obtained by slightly perturbing (perturbed mass within 0.1% of the unperturbed mass) S-branch stars. They reach a peak and then drop down at the approach of the maximum mass allowed for a given Λ signaling a transition from stability to instability. The frequencies for a given mass for higher Λ stars are lower than those for lower Λ as a result of their increased size. However, their overall maximum frequencies could get bigger than for lower Λ stars because of their increase in maximum mass. As can be seen $\Lambda=5$ and $\Lambda=10$ stars have higher maximum frequencies than do $\Lambda=0$ stars. As the stars get very much larger the maximum comes down as shown in the figure. $\Lambda=30$ stars have lower maximum frequency than $\Lambda=15$ stars which have lower maximal frequency of oscillation than do $\Lambda=10$ stars. (b) The highly perturbed $\Lambda=10$ S-branch star of Fig. 3 has an oscillation frequency below the $\Lambda=10$ solid line. Its movement towards the solid line is shown through points $P1$, $P2$ and $P3$ corresponding to times 0, 1200, and 4800 respectively.

shows the behavior of the radial metric in time as a function of radius. It oscillates about the final S-branch configuration that it will settle into. This final state is shown on the plot as a dark line. Figure 5(b) shows the maximum radial metric as a function of time. The star initially expands rapidly as it moves to the S-branch. This can be seen from the sharp drop in the radial metric. Once it moves to the stable branch, it oscillates about the new configuration that it is going to settle to. Figure 5(c) shows the mass of the star as a function of time. It loses mass at each expansion, losing less and less mass at each subsequent expansion, and the curve gets smoother and smoother as it prepares to settle to its final state.

Figure 6, which shows the oscillation frequency as a function of mass for $\Lambda=30$, can be used to predict the end point of migration. Points $Q1$, $Q2$, $Q3$ and $Q4$ show the migration of this star. These correspond to times of 500, 1000, 2000 and 3500. The oscillation is clearly damping out. The final configuration it is expected to settle down to is shown as a dot and corresponds to a stable star of central density $\sigma(0)=0.0817$ with a mass of $1.037m_{Pl}^2/m$. This example is typical of a number of simulations of U-branch ground state configurations with self-coupling.

For higher central density stars on the U-branch, the mass versus central density curve has a second, gentler peak, similar to the white dwarf neutron star situation. One might suspect that this corresponds to another stable and unstable branch respectively. However, we find that configurations on both sides of the peak are unstable. These configurations always disperse upon perturbation, consistent with the fact that they have $M>Nm$, where M was the mass of the star and Nm was the number of bosons multiplied by the mass of a boson.

In summary ground state configurations of boson stars with self-coupling have stable (S) and unstable (U) branches just like boson stars without self-coupling. The stable configurations have very specific quasinormal modes of oscillation. The addition of a self-coupling term serves to increase their mass. The cases considered so far correspond to $\Lambda\sim10^2$ or less. The Appendix deals with very high Λ stars which need a different technique due to the very different time scales involved in these evolutions.

IV. EVOLUTIONS OF EXCITED STATES

Excited states of boson stars have field configurations characterized by nodes. The first excited state has one node,

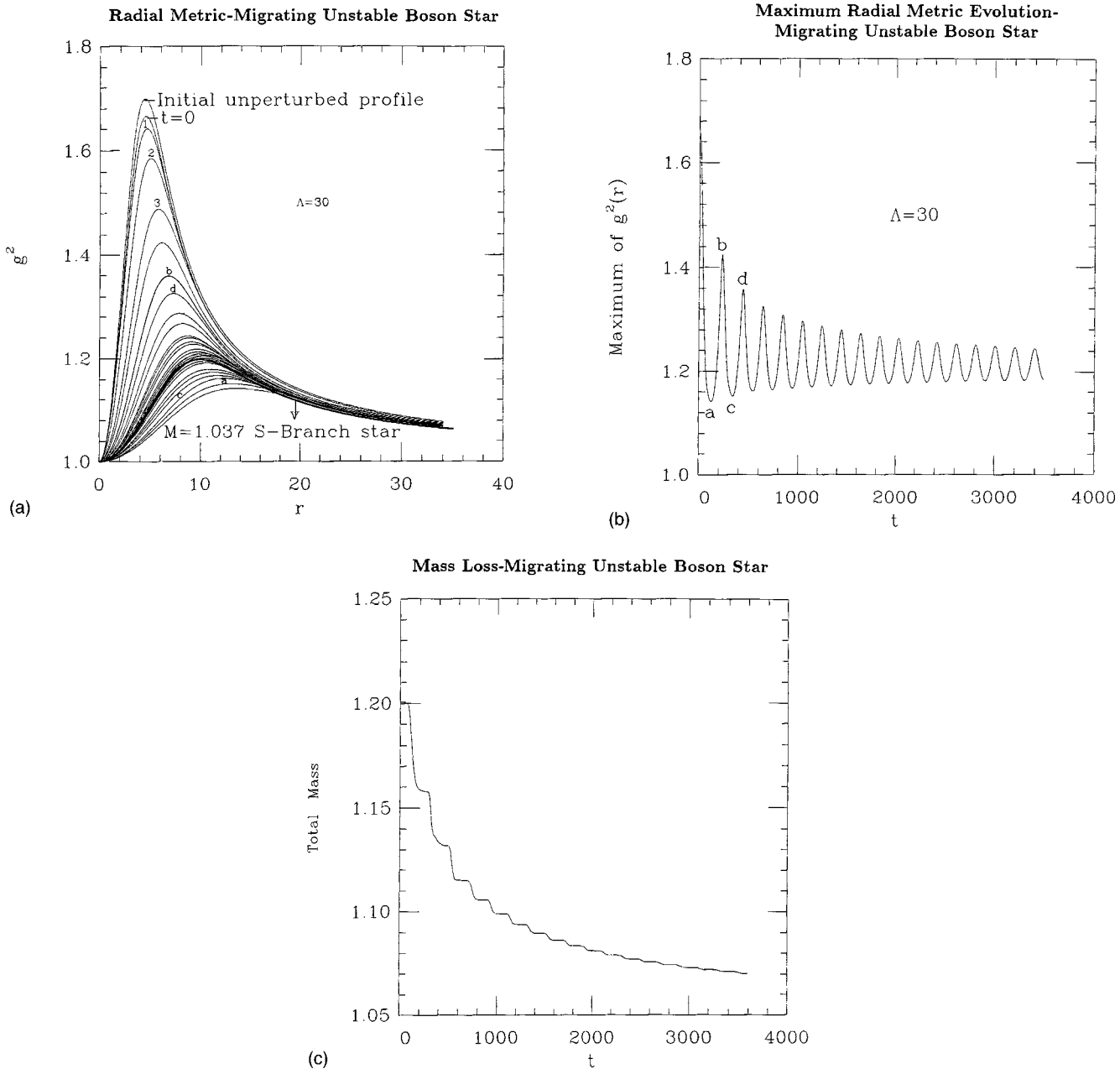

FIG. 5. (a) The radial metric $g^2 = g_{rr}$ of a perturbed U-branch ground state star is shown at various times. The curves 1,2,3,a,b,c,d correspond to times $t = 10$, 20, 30, 340, 440, 540 and 640. The unperturbed star has a central density $\sigma(0) = 0.23$ and a self-coupling parameter $\Lambda = 30$. The initial equilibrium metric configuration is also shown. The overall field density of this star has been lowered by about 10%. The $t = 0$ curve corresponds to the initial perturbed radial metric. In the asymptotic region g^2 is not oscillating but monotonically decreasing due to the mass loss. (b) The maximum value of the radial metric is plotted as a function of time. The initial sharp drop in the radial metric signifies the expansion of the star as it proceeds to the stable branch. There it oscillates about the new stable configuration that it is going to settle to. This corresponds to a star of mass $M = 1.037 m_{Pl}^2/m$ [whose metric configuration has been shown in figure (a) as a dark line]. The points a and c correspond to two minima in the peak of g_{rr} which occur when the core of the star reaches its local maximum size. Likewise the maxima in the peak of g_{rr} at b and d correspond to the core of the star reaching its local minimum size. (c) The mass is plotted against time. The mass loss through scalar radiation at each expansion of the core (corresponding to the maximum radial metric reaching a minimum) decreases in time as the oscillations damp out.

the second has two and so on. Studying their stability and the time scale of decay is important in determining the likelihood of finding them in nature.

The mass profiles of excited state boson stars are similar to ground state stars. Figure 7 shows the mass versus central density curves for ground, first and second excited states of boson stars without self-coupling. The maximum mass increases with the number of nodes as expected. The similarity of mass profiles of excited boson stars to their ground state counterparts might lead one to expect stable and unstable

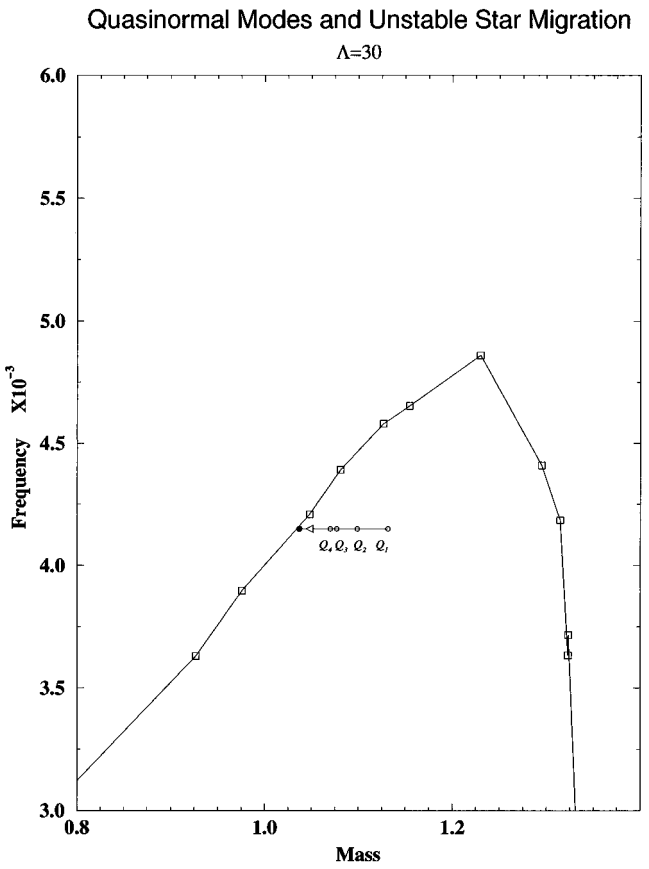

FIG. 6. The migration of the U-branch star considered in Fig. 5 is shown after the star has moved to the S-branch. Points $Q1$, $Q2$, $Q3$ and $Q4$ correspond to times 500, 1000, 2000 and 3500 respectively. Here too the mass loss decreases in time and the star finally settles to a stable configuration.

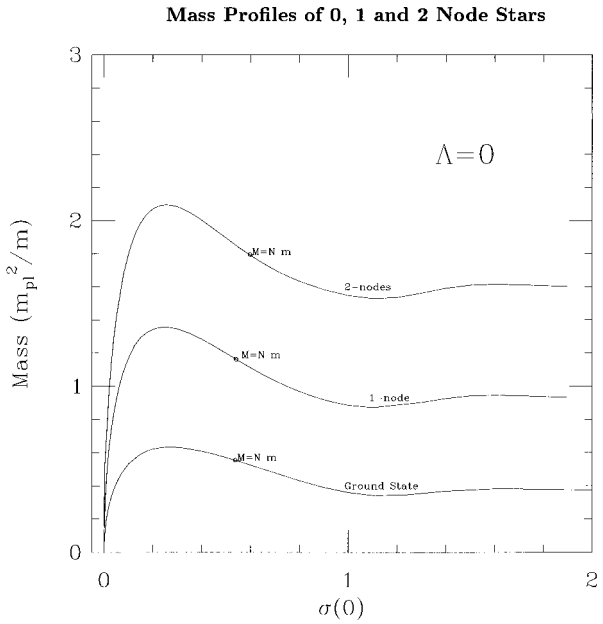

FIG. 7. The masses of 0-node, 1-node and 2-node boson stars without self-coupling are plotted as a function of central density. The maximum mass of 1-node stars is $1.356m_{Pl}^2/m$ while the maximum mass for 2-node stars is expectedly greater at $2.095m_{Pl}^2/m$. The profiles are deceptively similar to their ground state counterpart. Excited state stars are inherently unstable irrespective of the branch they lie on, unlike ground state stars that can be termed stable or unstable depending on whether they lie on the branch to the left of the maximum mass or to the right respectively.

configurations to the left and right of the maximum mass respectively in analogy with ground state configurations. However, our numerical studies show that the excited boson star configurations on both sides of the peak are inherently unstable except that the time scales for instability are different. If they cannot lose enough mass to go to the ground state, they become black holes or totally disperse. This occurs even if no explicit perturbations are put in the numerical evolution other than those introduced by the finite differencing error in the numerical integration. We have also carried out perturbations that correspond to more scalar particles falling on to the star or those that decrease the scalar field strength at the center point corresponding to scalar particles decaying through some channels [5]. The instability shows up in all cases studied. We note that this instability is *not* in contradiction with the result of [4], which concluded that S branch excited states are stable under infinitesimal perturbations that strictly conserve M and N (where M is the mass of the star, N the number of bosons and m the boson mass). Our result of instability under generic perturbation is consistent with the studies of $\Lambda=0$ stars under infinitesimal perturbation [12]. The presence of a self-coupling term increases the time scale of instability but the essential pattern remains the same. In the following we will first give a detailed account of the dynamical evolution and carry out a study of the instability time scales.

Excited state stars with masses less than the maximum mass of a *ground* state configuration always form ground state stable configurations. In fact even stars with masses somewhat greater than this can lose enough mass during their evolution so as to go to the ground state. Figure 8(a) shows a perturbed 1-node star whose mass has been reduced by about 8% to $0.9m_{Pl}^2/m$ by a perturbation making a transition to the ground state although the mass is greater than the maximum ground state mass of $0.633m_{Pl}^2/m$. A substantial amount of scalar radiation is emitted in the dynamical evolution, which brings the mass below the critical value. The evolution of the radial metric function is shown. Although the plot is shown only to a radius $r=100$, the actual evolution was carried out to $r=300$. The two peaks at $t=0$ are indicative of a first excited state. One of the peaks disappears gradually as the star goes to the ground state. The star then oscillates about the ground state configuration that it will finally settle into. In Fig. 8(b) we show a 3 node configuration with a total mass of $0.92m_{Pl}^2/m$, going to the ground state after radiation by scalar waves carries off the excess mass and kinetic energy. We have plotted the density function against the radius and time of evolution. By the density function we mean density ρ multiplied by an r^2 factor which is the mass per dr at radius r. ρr^2 has $n+1$ maxima for an n node star and hence here we have 4 sets of lines initially. At the end of the simulation, we see that it

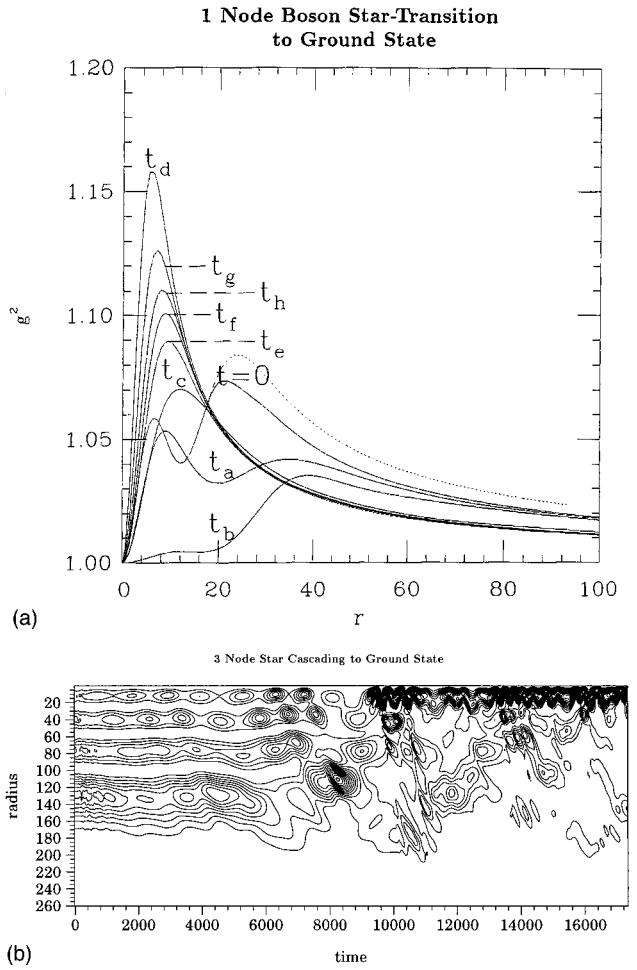

FIG. 8. (a) The transition of a first excited state star to the ground state is shown. Here the radial metric is plotted against radius for various times starting from $t=0$ and then for $t_a=250$, $t_b=500$, $t_c=1245$, $t_d=4000$, $t_e=5000$, $t_f=5505$, $t_g=6000$ and $t_h=6370$. The initial unperturbed and perturbed configurations are shown. (The perturbed configuration has the lower second peak.) The initial mass of the star was $M=.901m_{Pl}^2/m$ after perturbation. The radial metric initially has two peaks indicative of a 1-node configuration. As the star evolves and goes to the ground state one peak disappears. This can be seen in the curves from t_c-t_h. Once in the ground state it oscillates and finally settles into a stable ground state configuration. (b) The transition of a 3 node configuration of mass $0.91m_{Pl}^2/m$. This star loses enough mass during the course of its evolution to move to the ground state.

settles down to a ground state configuration with small oscillations with ever decreasing amplitude. For these simulations of low central density stars we put in an explicit perturbation to the equilibrium configuration since the instability time scales are extremely long without that.

For stars with higher central density, there is a critical density above which the stars cannot lose enough mass to go to the ground state but collapse to black holes. In our numerical simulation for one node stars this critical density is $\sigma(0)=\sigma_2=0.048$. As the central density is increased the kinetic energy of the highly compressed initial equilibrium configuration is increased and the star first expands before the eventual collapse to a black hole. As the central density further increases towards the $M=Nm$ point the expansion phase becomes longer. In Fig. 9(a) we show the density function ($\rho\times r^2$) against radius at various times for 4 configurations [an S branch configuration with $\sigma(0)=0.1$ and three U branch configurations of central densities $\sigma(0)=0.3$, $\sigma(0)=0.4$ and $\sigma(0)=0.5$]. The initial configurations are the equilibrium ones without any explicit perturbation (except those introduced by the discretization used in the numerical simulations). The first frame shows the S branch star radiating a little as it makes a transition to the ground state. However, it cannot sustain this state for long and it collapses to a black hole. The time of decay decreases in the case of a U branch stars of central density 0.3 and 0.4. However, for the $\sigma(0)=0.5$ star the star is clearly more dispersive than the previous ones. It goes through an expansion phase initially although it finally collapses to a black hole. Configurations with $\sigma(0)>0.54$ have $M>Nm$. They do not collapse to black holes but disperse to infinity.

Next we turn to a study of instability time scales. In simulations where a black hole will form, the imminent development of an apparent horizon leads to a rapid collapse of the lapse due to the polar slicing used in the evolution. We take the time of collapse of the lapse at the origin to $\sim 10^{-6}$ of its initial central value to be the approximate time for formation of the black hole. Figure 9(b) shows this time scale for a 1-node star without self-coupling. We plot the decay time scales of first excited state stars as a function of central field density. Again no explicit perturbation is applied in these evolutions other than the discretization error in the simulation. In order to make a fair comparison of the time scale due to such a perturbation we cover the radius of the star in all cases by the same number of grid points. The maximum ground state mass for stars without self-coupling is around $.633m_{Pl}^2/m$. This corresponds to a central density of $\sigma_1=0.021$ for a 1-node star. We described earlier that stars with central densities below $\sigma_2=0.048$ (mass of $0.91m_{Pl}^2/m$) lose enough mass and move to the ground state. Beyond that and up to the $M=Nm$ point they collapse to black holes, while stars with $M>Nm$ corresponding to a central field density of $\sigma(0)>0.541$ disperse to infinity. The time by which collapse takes place to a black hole decreases with increasing central density along the S branch. This trend continues for a while into the U branch (starting at $\sigma=0.25$ until $\sigma\sim 0.4$) but as one approaches the $M=Nm$ point the stars lose a significant amount of matter to infinity before they collapse to black holes and evolve on a longer time scale. For example a star of central density 0.5 has an initial radius of $r\sim 9$. (The radius of the star is defined as the radius which contains 95% of the mass of the star.) Its radius increases to as much as 115, more than an order of magnitude, before it starts collapsing. Dispersion time scales of a couple of stars for $M>Nm$ which disperse to infinity (instead of collapsing to a black hole) are also shown on the figure. To give a sense of the instability time scales of these configurations we take the time scale to be the time by which these stars disperse to 10 times their original radii. This time drops drastically for stars with $M\gg Nm$.

Next we turn to the case of $\Lambda\neq 0$. Figure 10(a) shows

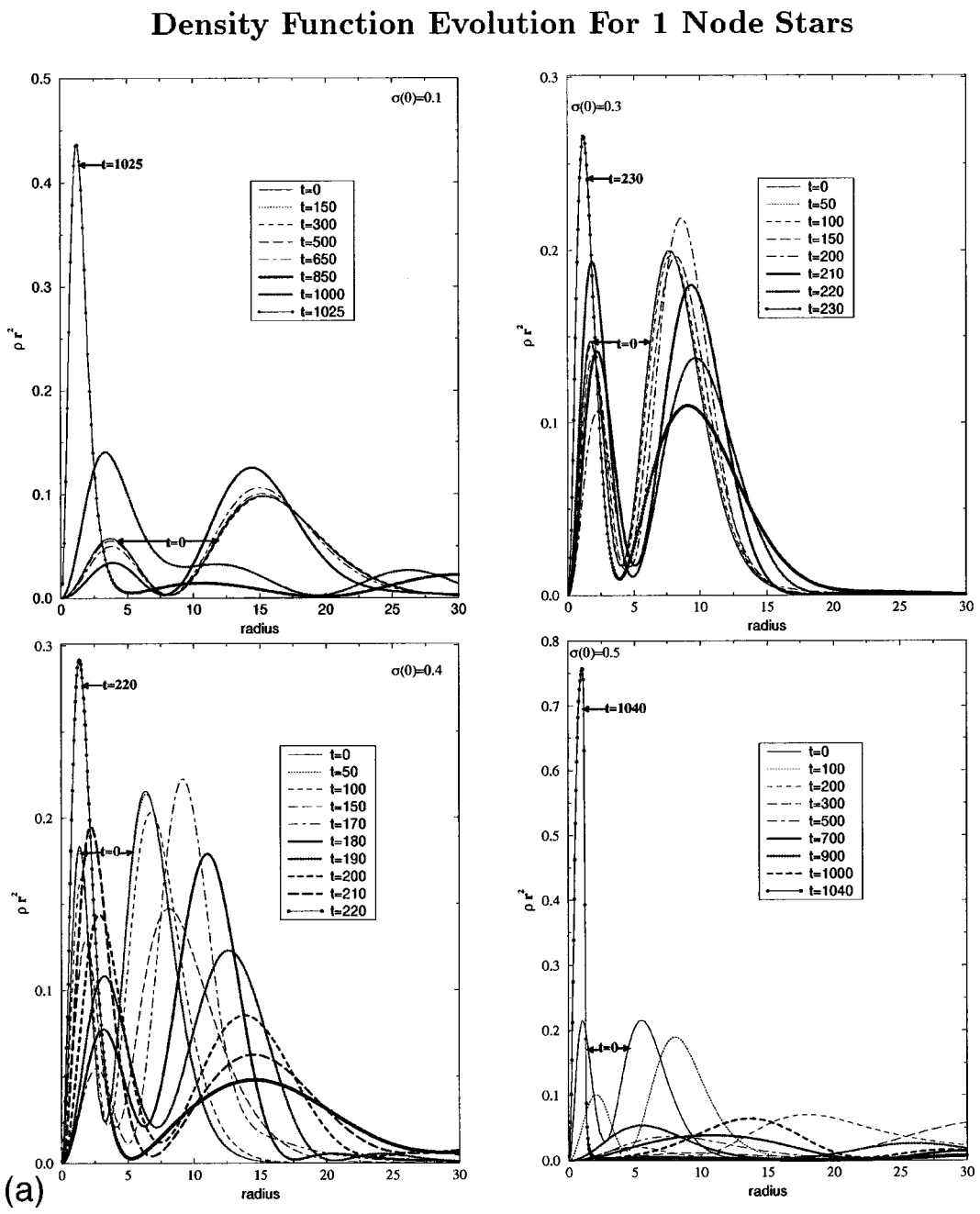

FIG. 9. (a) A comparison of the manner of black hole formation of four excited state configurations. The first frame is an *S* branch star of central density $\sigma(0)=0.1$ that tries to go to the ground state but fails to. As the central density increases decays to black holes occur on a shorter time scale. A plot of the collapse of a *U* branch of central density $\sigma(0)=0.3$ is shown in the next frame. Stars get more dispersive as one moves farther along the *U* branch. A star of central density 0.4 shown in the third frame has a decay time close to the previous one. Decay times then start to increase. A star of central density 0.5 close to the $M=Nm$ point $[\sim\sigma(0)=0.541]$ disperses to over 10 times its radius before collapsing to a black hole. (b) The decay time to black holes is plotted as a function of central density, for one node configurations (first excited states), of boson stars without self-coupling. Perturbations are only due to the finite differencing effects of the numerical scheme. To make the comparisons meaningful the 95% mass radius (which is our definition for radius of a star) of every configuration considered was covered by the same number of grid points. Configurations for which the central density $\sigma(0)<\sigma_2$ move to the ground state. This value of the critical density $\sigma_2=0.048$ corresponds to a mass $M=0.91m_{Pl}^2/m$. $\sigma_1=0.021$ is the value of the central density corresponding to a mass $M=0.633m_{Pl}^2/m$, which is the maximum mass of a ground state boson star. The decay time decreases with increasing $\sigma(0)$ and this continues even for $\sigma(0)>0.25$ which is the point of transition from the *S*-branch to the *U*-branch. The decay time then starts to increase as one approaches the $M=Nm$ point corresponding to a central density $\sigma(0)=0.541$, beyond which the stars disperse to infinity rather than become black holes. The dispersion times of two such stars to 10 times their original radius (95% mass radius) are also shown in the figure.

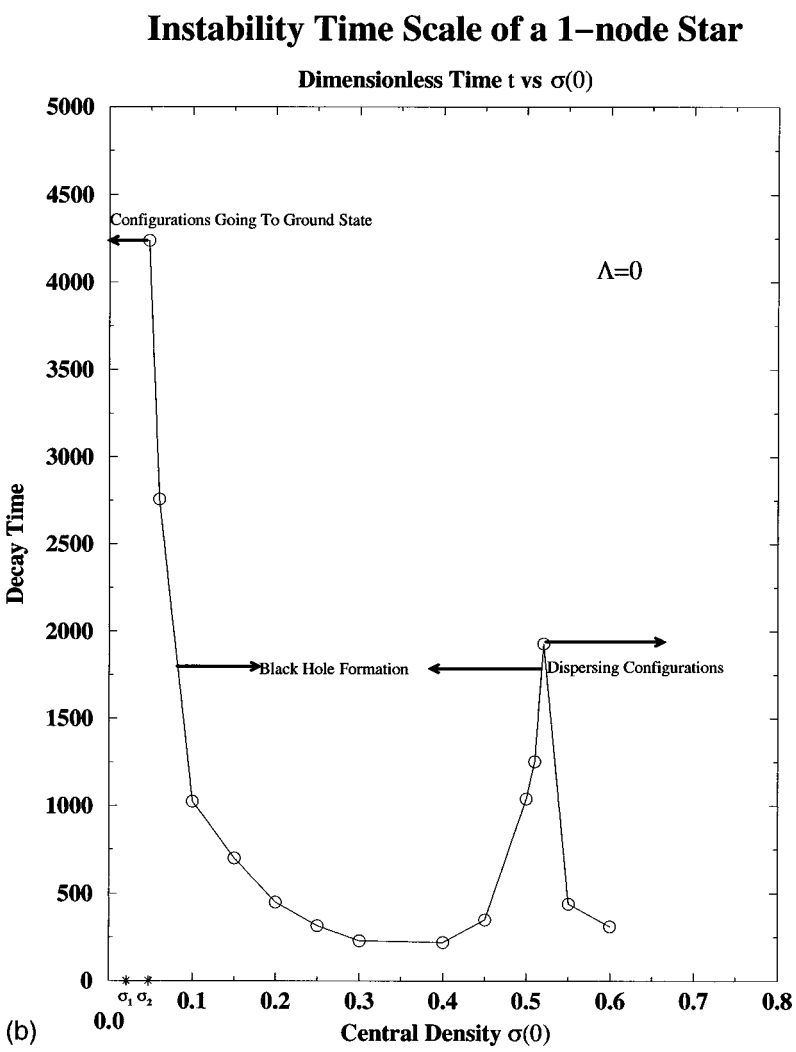

FIG. 9 (*Continued*).

black hole formation for a $\Lambda=30$ star in the first excited state, with a central density $\sigma(0)=0.1$. This star had an initial radius of about 20.7 where the radius is again defined as that containing 95% of the mass. The lapse finally collapses to zero, indicating that an apparent horizon is about to form. The time scale of collapse to the black hole was around 1985 compared to a time scale of less than 800 for a $\sigma(0)=0.122$ star of similar radius without self-coupling which is shown in Fig. 10(b). This is to be expected as the Λ term represents a repulsive force. The time is again determined by the lapse collapsing to 10^{-6} of its original value at $r=0$.

We now turn to the evolution of a highly excited state. In Fig. 11(a) we show the initial field configuration of a star containing 5 nodes. For a five node star the density has a central maximum, and then five local maxima, each subsequent one smaller than the one preceding it. This star is then evolved without any perturbation except those introduced by the discretization error of the numerical evolution. In Fig. 11(b) we show a contour plot of the evolution of the density function in time. ρr^2 has $n+1$ maxima for an n node star and hence here we initially have 6 sets of lines centered at dimensionless $r=5$, 13, 35, 52 and 75 respectively. This star has central density $\sigma(0)=0.075$ and it collapses to a black hole after a long evolution. In the process we see intermediate states with fewer numbers of nodes. For comparison in Fig. 11(c) show a contour plot for the 5 node star up to a time of $t=1000$ at which time it has decayed into a four node state, against the equilibrium density function of a 4 node star with central density $\sigma=0.06$. Very clearly the maxima are at similar radii (although the sizes of the peaks are somewhat different).

This feature of nodes disappearing and the star cascading through lower excited states is characteristic of the decay of higher excited states of boson stars. Although in this case and at this time the decaying star is close to a specific lower excited state, in general the decaying star is roughly a combination of lower excited configurations. This is similar to the decay of atoms in excited states. However, we note that for the ''gravitational atom'' [3] there is no exact superposition due to the intrinsic non-linearity of the system.

V. CONCLUSION

In the first paper in this series, the behavior of boson star ground state configurations under various perturbations was

reported. In this paper the study has been extended to include boson stars of self-interacting fields and also the behavior of boson stars in the excited state.

The self-coupling term is important as it can have dramatic effects on the mass of the boson stars [6], leading to boson stars of the order of a solar mass. The mass profile retains the features of boson stars without self-coupling, having a central maximum with a stable branch and an unstable branch. All configurations to the left of the central maximum in the mass vs central density curve (see Fig. 1) are stable. Under small perturbations they have very specific quasinormal modes of oscillation as seen in Figs. 4 and 6 and under perturbations they settle down to new configurations on the same branch. Configurations that lie on the unstable or *U*-branch either migrate to new configurations on the *S*-branch or collapse to black holes, when perturbed. These are characteristics shared by boson stars with or without self-coupling.

Excited states are configurations with nodes. The field of an n^{th} excited state star has n nodes and its radial metric has $n+1$ peaks. Their mass profiles are similar to the profiles of boson stars in the ground state, which makes it appear as if they have a stable and an unstable branch of configurations. However, irrespective of which branch they lie on, excited boson stars are unstable with different instability time scales. Low density excited stars having masses close to ground state configurations will form ground state boson stars after evolution. Denser configurations form black holes with the decay time decreasing with increasing central density until one approaches the density corresponding to zero binding energy. As the central density approaches this central density the kinetic energy of the star starts to increase as it becomes more dispersive. It still collapses to a black hole but on a larger time scale. Beyond this point for densities corresponding to positive binding energy the stars disperse to infinity. We studied the time scales of their instability in Fig. 9.

An interesting feature in the collapse of excited state boson stars is that they cascade through intermediate states, during this process, rather like atoms transiting from excited states to the ground state, suggesting that boson stars behave in some ways like gravitational atoms [3]. However, an investigation of the possible decay channels (selection rules) seems much more difficult (if at all possible or meaningful) here, due to the intrinsic nonlinearity of the theory. In this paper we have reported the evolutions of spherically symmetric configurations. We are currently extending the study to full 3D without spherical symmetry. The numerical study of 3D boson stars in addition to being an interesting physical problem is also a testbed for 3-dimensional numerical codes, which enable us to study compact self-gravitating objects without having to deal with hydrodynamic sources as in neutron stars and singularities as in the case of black holes. In particular we aim to study the general two body problem in relativity by evolving two 3-dimensional scalar field configurations. The inspiral coalescence of such systems could have interesting physical implications as the gravitational wave emitted does not sensitively depend on the internal structure of the compact objects until the late stages of coalescence. Studying the 1D behavior has been an important tool in test-

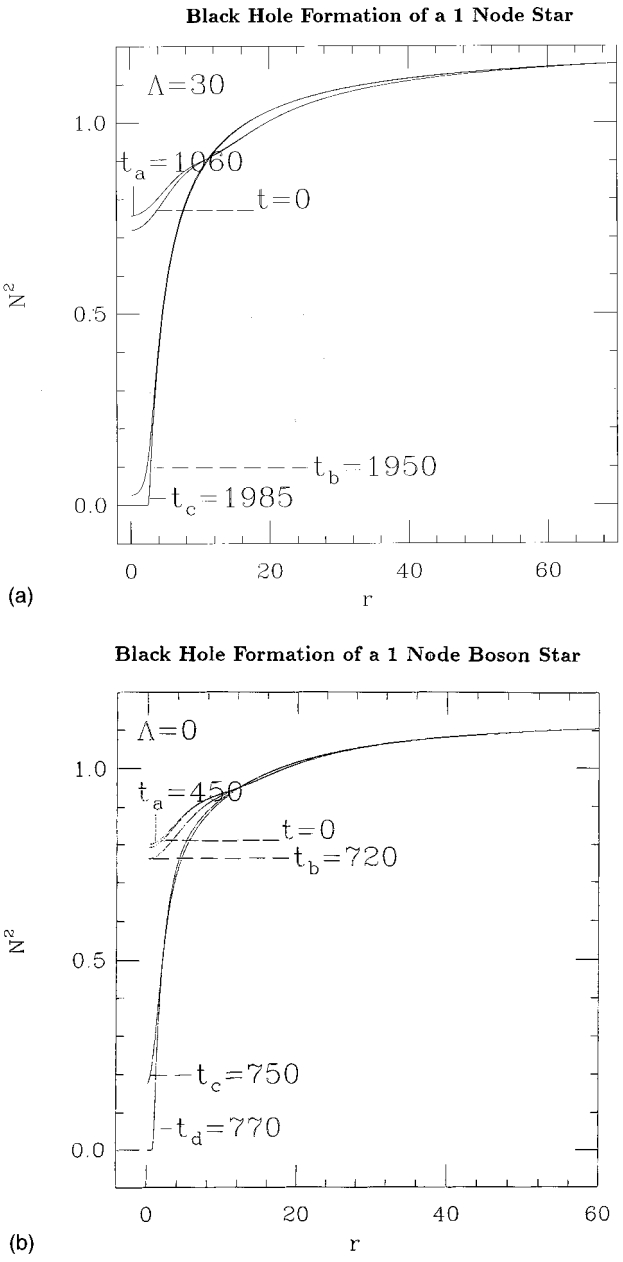

FIG. 10. (a) The evolution of the metric function $N^2=-g_{tt}$ for a $\Lambda=30$, $\sigma(0)=0.1$ boson star in the first excited state, without any explicit perturbation, is shown. The configuration lies on the *S*-branch and has an initial mass $M=1.743m_{Pl}^2/m$. The various time slices correspond to times $t=0$, $t_a=1060$, $t_b=1950$ and $t_c=1985$. The lapse function collapses as an apparent horizon is approached, signaling the formation of the black hole (indicative of an inherent instability of excited states). (b) The evolution of the metric function $N^2=-g_{tt}$ for a $\Lambda=0$, $\sigma(0)=0.122$ boson star in the first excited state, without any explicit perturbation, is shown. The configuration lies on the *S*-branch and has an initial mass $M=1.23m_{Pl}^2/m$. The various time slices correspond to times $t=0$, $t_a=450$, $t_b=720$, $t_c=750$ and $t_d=770$. This star has a radius of 20.7 which is about the same as that of the configuration in (a). Again, the lapse function collapses when an apparent horizon is approached, as a black hole is being formed. The time scale of collapse is much less than for the $\Lambda=30$ case in part (a).

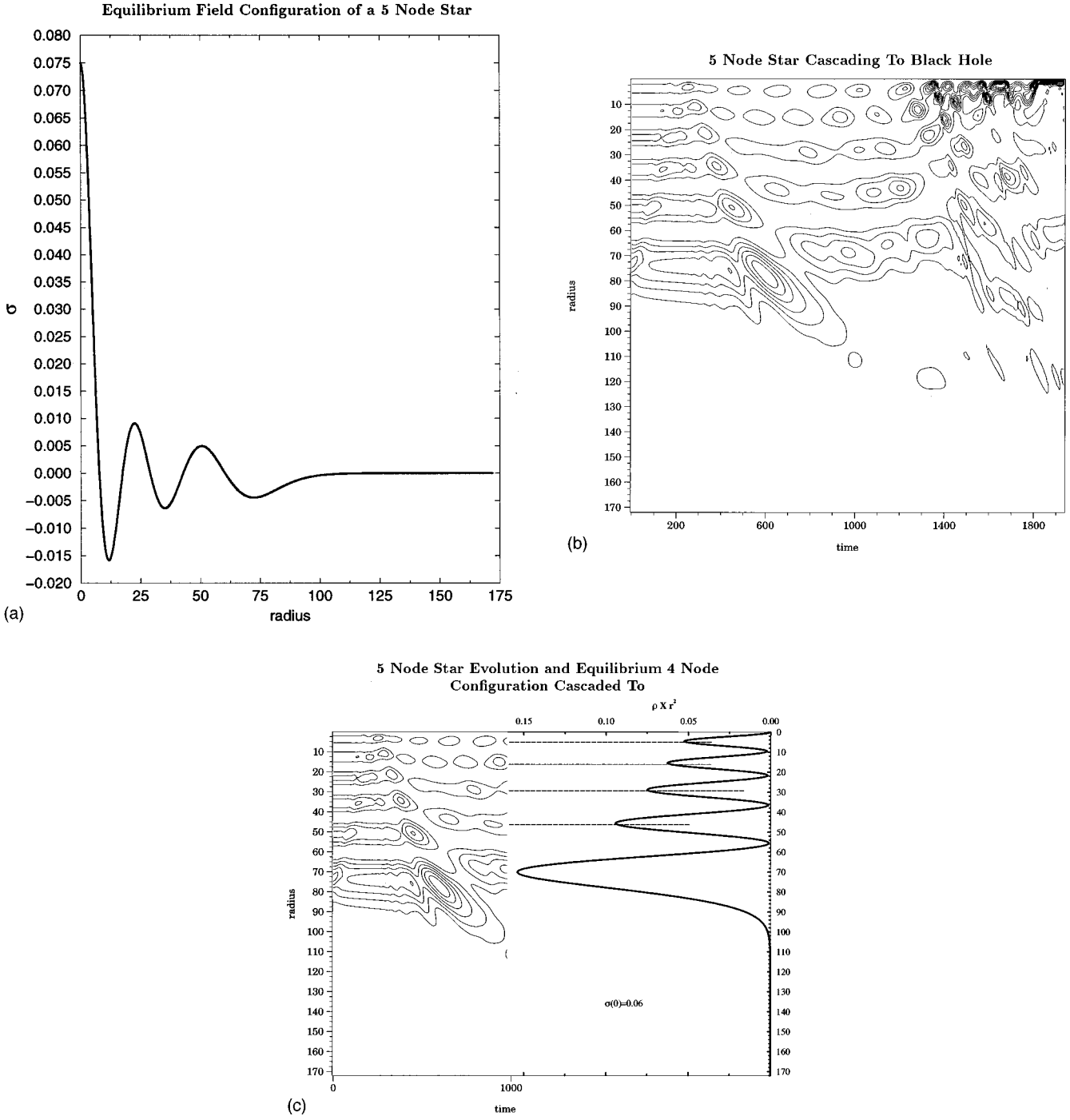

FIG. 11. (a) The initial field configuration of a 5-node star. The field has 5 nodes or extrema. The absolute value of each extremum is clearly smaller than the one preceding it. (b) A contour plot of a perturbed 5-node star that ends in a black hole showing $\rho \times r^2$ as a function of distance (vertical axis) and of time (horizontal axis) is shown. The density ρ is highest at the origin and has five other local maxima, each smaller than the previous one. The values of the maxima at the end are very small compared to the earlier ones, and to enhance the features $\rho \times r^2$ rather than just ρ is shown in the plots. Each set of lines represents the maxima of $\rho \times r^2$ and the number of lines in a set gives an indication of the height of the maximum. This particular configuration has a central density of $\sigma(0)=0.075$ and initial mass $M=3.07m_{Pl}^2/m$. This star cascades through an intermediate 4 node state (around $t=1000$) before proceeding to form a black hole. Cascades are characteristic of excited boson star decays similar to atoms in excited states going through intermediate states when transiting to the ground state. (c) The equilibrium density function of a 4 node star of central density $\sigma=0.06$ (right frame) is placed alongside the contour plot of the 5 node star described in (b) up to a time of $t=1000$ when it has gone into a 4 node state (left frame). This plot shows that the transition of the 5 node star is to a perturbed 4 node state close to the one shown in (c) before it continues its evolution to a black hole.

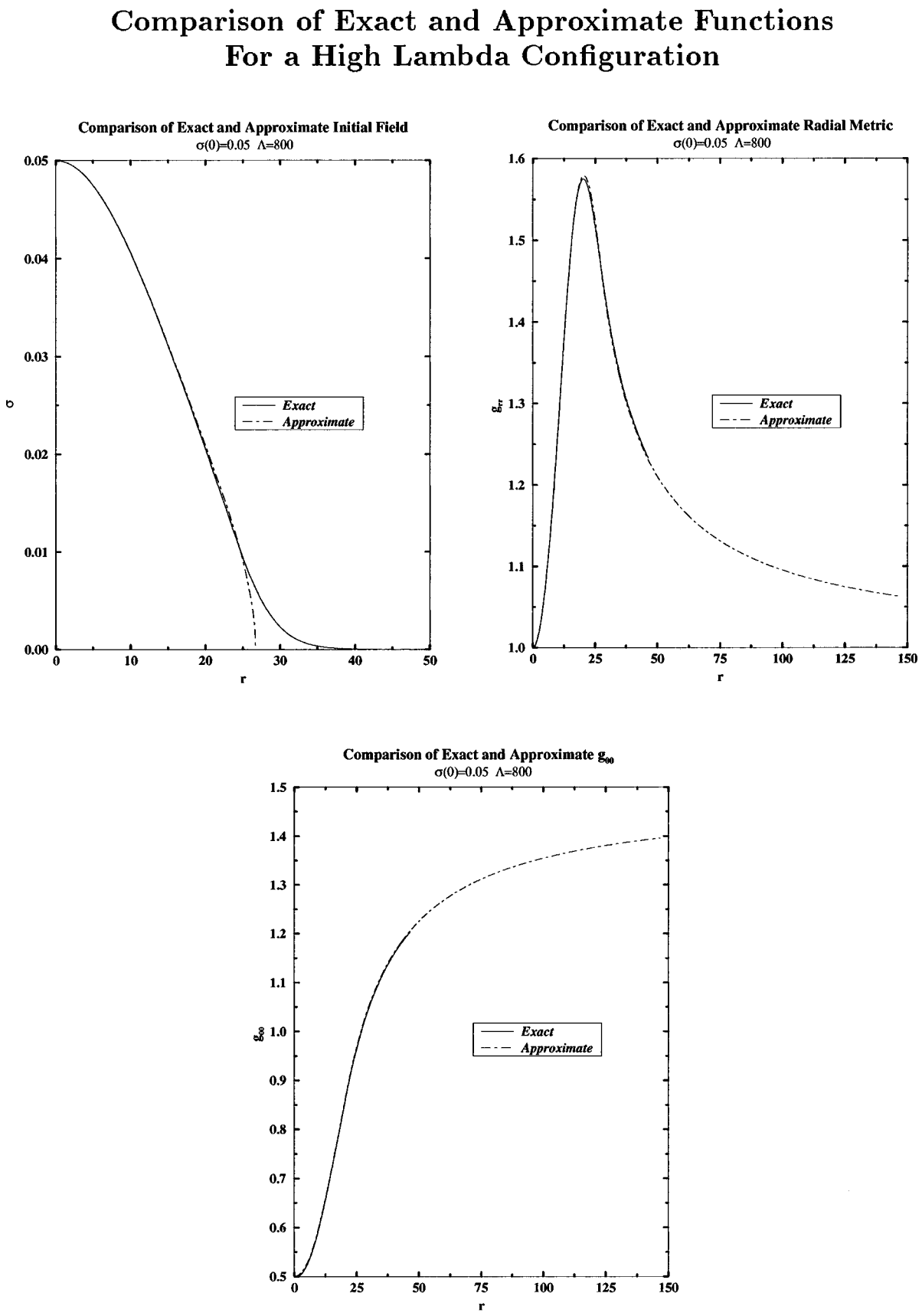

FIG. 12. The equilibrium profiles of a $\Lambda = 800$ star with central density $\sigma = 0.05$ derived from the high Λ approximate equations and the exact ones are compared. A Schwarzschild exterior is attached to the approximate solution after the field vanishes. The three plots show the field σ, g_{rr} and g_{00} respectively. Clearly, the approximation matches the exact solution very well.

ing our 3D codes, providing testbeds in the spherically symmetric limit.

ACKNOWLEDGMENTS

We are happy to acknowledge helpful discussions with Greg Daues and Malcolm Tobias. This research is supported in part by the McDonnell Center for Space Sciences, the Institute of Mathematical Science of the Chinese University of Hong Kong, the NSF Supercomputing Meta Center (MCA935025), National Science Foundation (Phy 96-00507), and NSF (Phy-07882).

APPENDIX: HIGH Λ CASE—EQUILIBRIUM CONFIGURATION AND QUASINORMAL MODE DETERMINATION

While calculating the eigenvalue for the equilibrium boson star, it is found that it gets increasingly difficult to calculate the eigenvalue as the value of Λ gets large because we are faced with a set of stiff equations. There are two scales to the problem: a scale of slow variation of the field inside a certain radius related to Λ followed by rapid decay outside it. This makes an effective surface layer to the star, making it more similar to neutron stars. It turns out that the large Λ limit can be treated using a set of approximate equations that are exact in the $\Lambda=\infty$ limit [6]. By making the change of variables

$$\bar{r}=r/\sqrt{\Lambda}, \quad \bar{\sigma}=\sqrt{\Lambda}\sigma \tag{A1}$$

the equilibrium equations reduce to

$$\frac{1}{\Lambda}\bar{\sigma}''=-\frac{1}{\Lambda}\left[\frac{1}{\bar{r}}+\frac{g^2}{\bar{r}}-\bar{r}g^2\bar{\sigma}_0^2\right]\bar{\sigma}'-\frac{1}{\sqrt{\Lambda}}\left[\frac{1}{N^2}-1\right]\bar{\sigma}_0 g^2 + \frac{1}{\sqrt{\Lambda}}(g^2\bar{\sigma}_0^3) \tag{A2}$$

$$g'=\frac{1}{2}\left[\frac{g}{\bar{r}}-\frac{g^3}{\bar{r}}+\bar{\sigma}_0^2\bar{r}g^3\left[1+\frac{1}{N^2}\right]+\frac{1}{\sqrt{\Lambda}}\bar{r}g\bar{\sigma}_0'^2 + \frac{1}{2}(g^3\bar{r}\bar{\sigma}_0^4)\right] \tag{A3}$$

$$N'=\frac{1}{2}\left[-\frac{N}{\bar{r}}+\frac{Ng^2}{\bar{r}}+\frac{\bar{r}g^2\bar{\sigma}_0^2}{N}(1-N^2)+\frac{1}{\sqrt{\Lambda}}\bar{r}N\bar{\sigma}_0'^2 - \frac{1}{2}g^2N\bar{r}\bar{\sigma}_0^4\right], \tag{A4}$$

where the primes refer to differentiation with respect to $\bar{r}$. In the limit of $\Lambda=\infty$, one can keep terms to leading order in $1/\sqrt{\Lambda}$ in Eqs. (A2)–(A4). In particular Eq. (A2) reduces to

$$N=(\bar{\sigma}^2+1)^{-1/2}. \tag{A5}$$

However, we note that this is valid only for a ground state configuration. For a state with nodes it would not be reasonable to neglect derivative terms compared to terms proportional to $\bar{\sigma}$, which is zero at a node.

To get an estimate of the accuracy of the high Λ approximation, we compare the solution using the approximate equation for high Λ to the brute force numerical solution of the complete set of equations, for a $\Lambda=800$, $\sigma=0.05$ boson star in the ground state in Fig. 12. The agreement of the fields is quite good until the outer region where the approximate equations cause the field to abruptly fall to zero. Comparisons of the radial metric and the lapse are also shown. In the $\Lambda=\infty$ limit the approximate equations are exact and the star really has an outer surface reminiscent of a neutron star. In fact, an equation of state can be written [6]. In Fig. 13 the mass and particle number versus central density $\bar{\sigma}$ for high Λ stars is shown. One expects as in the case of other ground state configurations that the configurations with $M>N_p m$ disperse when perturbed while those on the U branch with $M<N_p m$ would be unstable and, if unable to migrate to the S branch under perturbations, would form black holes. (Here we use the symbol N_p for the particle number and not N so as not to confuse it with the lapse as both these functions figure prominently in the analysis that follows.) The particle number is calculated from the current J^0 and is given by

$$N_p=4\pi\int r^2\frac{g}{N}\omega\sigma^2 dr. \tag{A6}$$

Here $\dot{\sigma}$ has been replaced by $\omega\sigma$ and d^3r by $4\pi r^2 dr$ for the spherically symmetric case. In terms of the *bar* coordinates we see that $\bar{N}_p=\sqrt{\Lambda}N_p$.

TABLE I. The ratio of the QNM frequency for $\Lambda=1600$ to the QNM frequency for a given Λ is compared to $\Lambda^{0.5}/40$ (which is the predicted ratio for large Λ) for $\Lambda=1200$, 800 and 1600. The higher Λ values match better as expected. The initial central density is $\bar{\sigma}(0)=0.4$.

Λ	$1/f$	f_{1600}/f	$\sqrt{\frac{\Lambda}{1600}}$	Percent (%) error
1600	1220	1	1	
1200	1070	0.877	0.866	1.25
800	880	0.7213	0.707	1.9
600	770	0.6311	0.612	3

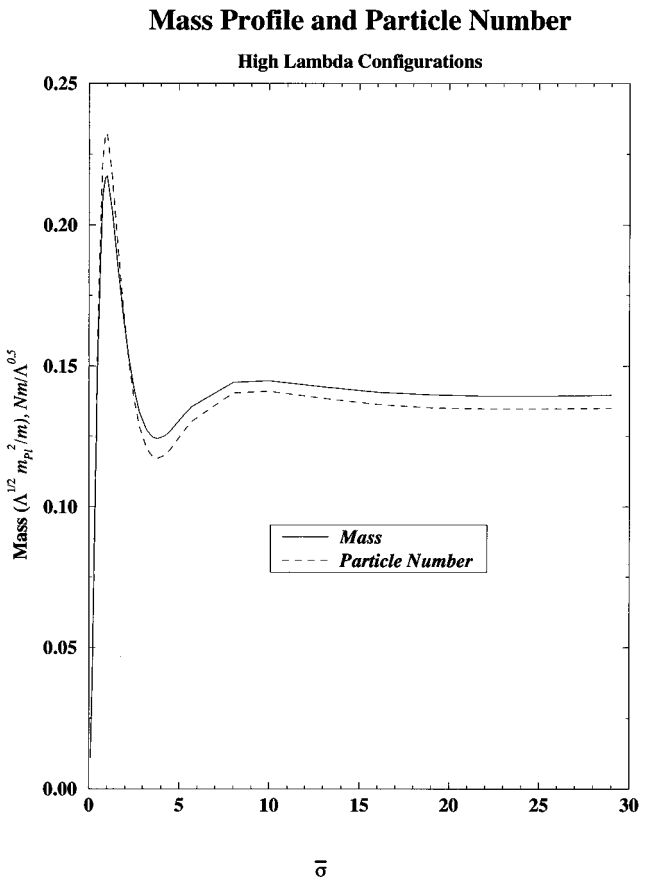

FIG. 13. The mass of a high Λ star generated from the approximate equations is plotted as a function of $\bar{\sigma}$ ($\sigma/\Lambda^{1/2}$). It shows the same basic structure as the profiles generated for low Λ using exact equations. The peak is at about $.22\Lambda^{1/2}m_{Pl}^2/m$ which means that to achieve $0.1M_\odot$ would take Λ of the order of 10^{38}, a very large star to evolve numerically. Also plotted is Nm (N is the particle number and m the mass of a boson). The crossing point of the two curves represents the transition from negative to positive binding energy.

Next we turn to the determination of the quasi-normal frequency (QNM) of the high Λ stars. In principle one could determine the QNM using the dynamical studies as performed for the $\Lambda=0$ case. However, the procedure is extremely computationally expensive. The scalar field has an inherent oscillation of about 2π and the evolution time steps must be small enough to resolve it. However, the code must run long enough to see a few metric oscillations in order to determine the quasinormal mode. As Λ gets large, the sizes of the stars also get large, leading to a lower frequency of oscillation. In order to determine the QNM we use instead the following perturbation analysis based on [8,11] but using our notation for lapse, fields, time, radius and self-coupling as defined in Sec. II.

We write the perturbed fields as

$$\sigma=(\sigma_1+\iota\sigma_2)e^{\iota\omega t},\quad g=g_0+\delta g,\quad N=N_0+\delta N \tag{A7}$$

where

$$\sigma_1=\sigma_0(r)[1+\delta\sigma_1(r,t)],\quad \sigma_2=\sigma_0(r)\,\delta\sigma_2(r,t). \tag{A8}$$

The Klein-Gordon equation can be written as

$$\sigma_1''+\left(\frac{2}{r}+\frac{N'}{N}-\frac{g'}{g}\right)\sigma_1'+g^2\left(\frac{1}{N^2}-1-\frac{1}{2}\Lambda\sigma_1^2\right)\sigma_1-\frac{g^2}{N^2}\,\ddot{\sigma}_1 + \frac{g^2}{N^2}\left(\frac{\dot{N}}{N}-\frac{\dot{g}}{g}\right)(\dot{\sigma}_1+\sigma_2)-2\frac{g^2}{N^2}\,\dot{\sigma}_2. \tag{A9}$$

The field σ_0 satisfies the equilibrium equation

$$\sigma_0''+\left(\frac{2}{r}+\frac{N_0'}{N}-\frac{g_0'}{g}\right)\sigma_0' + g_0^2\left(\frac{1}{2N_0^2}-1-\frac{\Lambda}{2}\sigma_1^2\right)\sigma_0-\frac{g_0^2}{N_0^2}\sigma_0=0. \tag{A10}$$

Expanding to first order perturbations using Eqs. (A9) and (A10) we get

$$\delta\sigma_1''+\left(\frac{2}{r}+\frac{N_0'}{N}-\frac{g_0'}{g}+2\frac{\sigma_0'}{\sigma_0}\right)\delta\sigma_1' -\frac{\sigma_0'}{\sigma_0}\left(\frac{g_0\delta g'-g_0'\delta g}{g_0^2}-\frac{N_0\delta N'-N_0'\delta N}{N_0^2}\right) -\frac{g_0^2}{N_0^2}(2\,\delta\dot{\sigma}_2+\delta\ddot{\sigma}_1)+\frac{2}{N_0^2}\left(g_0\delta g-\frac{\delta N}{N_0}\right) -2g_0\left(1+\frac{1}{2}\Lambda\sigma_0^2\right)\delta g-g_0^2\Lambda\sigma_0^2\delta\sigma_1=0. \tag{A11}$$

From

$$\mathbf{R}_{\mu\nu}-\frac{1}{2}g_{\mu\nu}\mathbf{R}=-8\pi G\mathbf{T}_{\mu\nu} \tag{A12}$$

and

$$T_{\mu\nu}=\sigma^*_{,\mu}\sigma_{,\nu}+\text{c.c.}-g_{\mu\nu}\left[g^{\alpha\beta}\sigma^*_{,\alpha}\sigma_{,\beta} -\left(1+\frac{1}{4}\Lambda\|\sigma\|^2\right)\|\sigma\|^2\right] \tag{A13}$$

(where $T_{\mu\nu}=4\pi G\mathbf{T}_{\mu\nu}$) we get the equations

$$\delta T_0^0=\frac{1}{2r^2}\left(\frac{2r\,\delta g}{g_0^3}\right)', \tag{A14}$$

$$\delta T_1^1=\frac{\delta g}{g_0^3}\left(\frac{1}{r^2}-2\frac{N_0''}{N_0}\right)-\frac{\delta N'}{rg_0^2N_0}-\frac{N_0'\delta N}{rg_0^2N^2}, \tag{A15}$$

and

$$\delta T_2^2=\frac{1}{2}\left\{\frac{2\delta g}{g_0}\left[\left(\frac{N_0'}{N_0}\right)^2+\frac{N_0N_0''-N_0'^2}{N_0^2}-\frac{N_0'g_0'}{N_0g_0}+\frac{1}{r}\left(\frac{N_0'}{N_0}-\frac{g_0'}{g_0}\right)\right]+\frac{1}{N_0^2g_0}\delta\ddot{g}\right.$$
$$-\frac{1}{g_0^2}\left[\frac{\delta N''}{N_0}-2\frac{N_0'}{N_0^2}\delta N'+\frac{N_0'}{N_0^2}\delta N-\frac{N_0'}{N_0g_0}\left(\delta g'-\frac{g_0'}{g_0}\delta g\right)-\frac{g_0'}{N_0g_0}\left(\delta N'-\frac{N_0'}{N_0}\delta N\right)\right.$$
$$\left.\left.+2\frac{N_0'}{N_0^2}\left(\delta N'-\frac{N_0'}{N_0}\delta N\right)+\frac{1}{r}\left(\frac{\delta N'}{N_0}-\frac{N_0'}{N_0^2}\delta N-\frac{\delta g'}{g_0}+\frac{g_0'}{g_0^2}\delta g\right)\right]\right\}, \tag{A16}$$

and the equations

$$\delta T_0^0=-\frac{2\sigma_0^2}{N_0^3}\delta N-\frac{2}{g_0^3}\sigma_0'^2\delta g+\delta\sigma_1\left[\frac{2}{N_0^2}\sigma_0^2+\frac{2}{g_0^2}\sigma_0'^2+2\left(1+\frac{1}{2}\Lambda\sigma_0^2\right)\sigma_0^2\right]-\delta\dot{\sigma}_2\frac{2}{N_0^2}\sigma_0^2+\frac{2}{g_0^2}\sigma_0\sigma_0'\delta\sigma_1', \tag{A17}$$

$$\delta T_1^1=-\delta T_0^0+4\sigma_0^2\delta\sigma_1, \tag{A18}$$

and

$$\delta T_2^2=-\frac{2}{N_0^3}\sigma_0^2\delta N-\frac{2}{g_0^3}\sigma_0'^2\delta g-\delta\sigma_1\left[\frac{2}{N_0^2}\sigma_0^2-\frac{2}{g_0^2}\sigma_0'^2-2\left(1+\frac{1}{2}\Lambda\sigma_0^2\right)\sigma_0^2\right]+\delta\dot{\sigma}_2\frac{2}{N_0^2}\sigma_0^2+\frac{2}{g_0^2}\sigma_0\sigma_0'\delta\sigma_1', \tag{A19}$$

respectively. Adding δT_0^0 to δT_1^1 we get

$$\left(\frac{\delta N'}{N_0}-\frac{N_0'\delta N}{N_0^2}-\frac{\delta g'}{g_0}+\frac{g'\delta g}{g_0^2}\right)=\frac{2}{g_0}\left[\frac{1}{r}+\left(\frac{N_0'}{N_0}-\frac{g_0'}{g_0}\right)\right]\delta g-4r\sigma_0^2(1+\Lambda\sigma_0^2)\delta\sigma_1. \tag{A20}$$

Substituting Eq. (A20) as well as for $\delta\dot{\sigma}_2$ from Eqs. (A16) and (A19) in Eq. (A11) we get

$$\delta\sigma_1''+\delta\sigma_1'\left(\frac{2}{r}+\frac{N_0'}{N_0}-\frac{g_0'}{g_0}\right)+\frac{1}{g_0^2r\sigma_0^2}(g_0\delta g'-g_0'\delta g)-\frac{g_0^2}{N_0^2}\delta\ddot{\sigma}_1+\frac{2\delta g}{g_0}\left[\frac{\sigma_0'^2}{\sigma_0}+\frac{g_0^2}{N_0^2}+\frac{1-2r\dfrac{g_0'}{g_0}}{2r^2\sigma_0^2}\right.$$
$$\left.-g_0^2\left(1+\frac{\Lambda\sigma_0^2}{2}\right)+\frac{\sigma_0'}{\sigma_0}\left(\frac{1}{r}+\frac{N_0'}{N_0}-\frac{g_0'}{g_0}\right)\right]-g_0^2\delta\sigma_1\left[\frac{1}{N_0^2}+\frac{1}{g_0^2}\left(\frac{\sigma_0'}{\sigma_0}\right)^2+(1+\Lambda\sigma_0^2)+2r\sigma_0'\sigma_0\left(1+\frac{\Lambda\sigma_0^2}{2}\right)\right]=0. \tag{A21}$$

Adding δT_0^0 to δT_2^2 and substituting in Eq. (A20) and its derivative we get

$$\frac{2}{g_0}\delta g''-\frac{2g_0}{N_0^2}\ddot{\delta g}+8\left[2\sigma_0\sigma_0'-r\left(1+\frac{1}{2}\Lambda\sigma_0^2\right)\sigma_0^2g_0^2\right]\delta\sigma_1'+8\left[2\sigma_0'^2-r\sigma_0^2g_0^2\left(1+\frac{1}{2}\Lambda\sigma_0^2\right)\left(\frac{2\sigma_0'}{\sigma_0}+\left\{\frac{2N_0'}{N_0}+\frac{g_0'}{g_0}\right\}\right)\right]\delta\sigma_1$$
$$-\left[\frac{4g_0'}{g_0^2}+\frac{6}{g_0}\left(\frac{N_0'}{N_0}-\frac{g_0'}{g_0}\right)\right]\delta g'+\frac{2\delta g}{g_0}\left[\frac{g_0''}{g_0}+2\left(\frac{g_0'}{g_0}\right)^2-3\frac{g_0'}{g_0}\left(\frac{N_0'}{N_0}-\frac{g_0'}{g_0}\right)\right.$$
$$\left.-8\sigma_0'^2-\frac{2}{r^2}-\frac{2}{g_0^2}(g_0g_0''-g_0'^2)+2\left(\frac{N_0'}{N_0}-\frac{g_0'}{g_0}\right)^2+\frac{2}{r}\left(\frac{2N_0'}{N_0}+\frac{g_0'}{g_0}\right)\right]=0. \tag{A22}$$

Using the expression for the particle number $N_p=\int_0^\infty d^3xJ^0\sqrt{g}$ where $J^0=\imath g^{00}(\phi_{,0}\phi^*-\text{c.c.})$ we get

$$\delta N_p=+4\pi\int_0^\infty drr^2\frac{g_0}{N_0}\sigma_0^2\mathbf{X}\left\{\frac{1}{g_0^2r\sigma_0^2}(g_0\delta g'-g_0'\delta g)+\frac{2\delta g}{g_0}\left(\frac{\sigma_0'^2}{\sigma_0}+\frac{1-2r\dfrac{g_0'}{g_0}}{2r^2\sigma_0^2}+\frac{g_0^2}{N_0^2}\right)+\frac{\sigma_0'}{\sigma_0}\delta\sigma'\right.$$
$$\left.-g_0^2\delta\sigma_1\left[\frac{1}{N_0^2}+\frac{1}{g_0^2}\left(\frac{\sigma_0'}{\sigma_0}\right)^2+\left(1+\frac{\Lambda}{2}\sigma_0^2\right)\right]\right\}. \tag{A23}$$

In terms of bar coordinates defined in the beginning of this section, Eq. (A21) becomes

$$\frac{1}{\Lambda^{1.5}}\delta\bar{\sigma}_1''+\frac{1}{\Lambda^{1.5}}\delta\bar{\sigma}_1'\left(\frac{2}{\bar{r}}+\frac{N_0'}{N_0}-\frac{g_0'}{g_0}\right)+\frac{1}{g_0^2\bar{r}\bar{\sigma}_0^2}(g_0\delta g'-g_0'\delta g)-\frac{1}{\Lambda^{0.5}}\frac{g_0^2}{N_0^2}\delta\bar{\sigma}_1$$

$$+\frac{2\delta g}{g_0}\left[\frac{1}{\Lambda}\left(\frac{\bar{\sigma}_0'}{\bar{\sigma}_0}\right)^2+\frac{g_0^2}{N_0^2}+\frac{1-2\bar{r}\dfrac{g_0'}{g_0}}{2\bar{r}^2\bar{\sigma}_0^2}-g_0^2\left(1+\frac{\bar{\sigma}_0^2}{2}\right)+\frac{1}{\Lambda}\frac{\bar{\sigma}_0'}{\bar{\sigma}_0}\left(\frac{1}{\bar{r}}+\frac{N_0'}{N_0}-\frac{g_0'}{g_0}\right)\right]$$

$$-\frac{1}{\Lambda^{0.5}}g_0^2\delta\bar{\sigma}_1\left[\frac{1}{N_0^2}+\frac{1}{\Lambda g_0^2}\left(\frac{\bar{\sigma}_0'}{\bar{\sigma}_0}\right)^2+(1+\bar{\sigma}_0^2)+\frac{1}{\Lambda}2\bar{r}\bar{\sigma}_0'\bar{\sigma}_0\left(1+\frac{\bar{\sigma}_0^2}{2}\right)\right]=0, \tag{A24}$$

and Eq. (A22) becomes

$$\frac{1}{\Lambda}\frac{2}{g_0}\delta g''-\frac{2g_0}{N^2}\ddot{\delta}g+\frac{8}{\Lambda^{1.5}}\left[\frac{2}{\Lambda}\bar{\sigma}_0\bar{\sigma}_0'-r\left(1+\frac{1}{2}\bar{\sigma}_0^2\right)\bar{\sigma}_0^2g_0^2\right]\delta\bar{\sigma}_1'+\frac{8}{\Lambda^{1.5}}\left\{\frac{2}{\Lambda}\bar{\sigma}_0'^2-r\left(1+\frac{1}{2}\bar{\sigma}_0^2\right)\bar{\sigma}_0^2g_0^2\left[\frac{2\bar{\sigma}_0'}{\bar{\sigma}_0}\right.\right.$$

$$\left.\left.+\left(\frac{2N_0'}{N_0}+\frac{g_0'}{g_0}\right)\right]\right\}\delta\bar{\sigma}_1-\frac{1}{\Lambda}\left[\frac{4g_0'}{g_0^2}+\frac{6}{g_0}\left(\frac{N_0'}{N_0}-\frac{g_0'}{g_0}\right)\right]\delta g'+\frac{2}{\Lambda g_0}\left[\frac{g_0''}{g_0}+2\left(\frac{g_0'}{g_0}\right)^2-3\frac{g_0'}{g_0}\left(\frac{N_0'}{N_0}-\frac{g_0'}{g_0}\right)\right.$$

$$\left.-\frac{8}{\Lambda}\bar{\sigma}_0'^2-\frac{2}{r^2}-\frac{2}{g_0^2}(g_0g_0''-g_0'^2)+2\left(\frac{N_0'}{N_0}-\frac{g_0'}{g_0}\right)^2+\frac{2}{r}\left(\frac{2N_0'}{N_0}+\frac{g_0'}{g_0}\right)\right]\delta g=0. \tag{A25}$$

Similarly Eq. (A23) becomes

$$\delta N_p=4\pi\int_0^\infty+drr^2\frac{g_0}{N_0}\bar{\sigma}_0^2\mathbf{X}\left\{\frac{1}{g_0^2\bar{r}\bar{\sigma}_0^2}(g_0\delta g'-g_0'\delta g)+\frac{2\delta g}{g_0}\left[\frac{1}{\Lambda}\left(\frac{\bar{\sigma}_0'}{\bar{\sigma}_0}\right)^2+\frac{1-2\bar{r}\dfrac{g_0'}{g_0}}{2\bar{r}^2\bar{\sigma}_0^2}\frac{g_0^2}{N_0^2}\right]+\frac{1}{\Lambda^{1.5}}\frac{\bar{\sigma}_0'}{\bar{\sigma}_0}\delta\bar{\sigma}'\right.$$

$$\left.-\frac{g_0^2}{\Lambda^0.5}\delta\bar{\sigma}_1\left[\frac{1}{N_0^2}+\frac{1}{g_0^2\Lambda}\left(\frac{\bar{\sigma}_0'}{\bar{\sigma}_0}\right)^2+\left(1+\frac{1}{2}\bar{\sigma}_0^2\right)\right]\right\}. \tag{A26}$$

Using $\delta N_p=0$ (charge conservation) which is appropriate for large Λ where δN_p is given by Eq. (A26) we get, on putting this in Eq. (A24),

$$\frac{1}{\Lambda^{1.5}}\delta\bar{\sigma}_1''+\frac{1}{\Lambda^{1.5}}\delta\bar{\sigma}_1'\left(\frac{2}{\bar{r}}+\frac{N_0'}{N_0}-\frac{g_0'}{g_0}\right)+-\frac{1}{\Lambda^{0.5}}\frac{g_0^2}{N_0^2}\delta\bar{\sigma}_1+\frac{2\delta g}{g_0}\left[-g_0^2\left(1+\frac{\bar{\sigma}_0^2}{2}\right)+\frac{1}{\Lambda}\frac{\bar{\sigma}_0'}{\bar{\sigma}_0}\left(\frac{1}{\bar{r}}+\frac{N_0'}{N_0}-\frac{g_0'}{g_0}\right)\right]$$

$$-\frac{1}{\Lambda^{0.5}}g_0^2\delta\bar{\sigma}_1\left[\frac{\bar{\sigma}_0^2}{2}+\frac{1}{\Lambda}2\bar{r}\bar{\sigma}_0'\bar{\sigma}_0\left(1+\frac{\bar{\sigma}_0^2}{2}\right)\right]-\frac{\bar{\sigma}_0'}{\Lambda^{1.5}\bar{\sigma}_0}\delta\bar{\sigma}=0. \tag{A27}$$

This equation suggests that δg goes like $1/\Lambda^{0.5}$. Writing $\ddot{\delta}g$ as $-\chi^2\delta g$ and $\ddot{\delta}\bar{\sigma}$ as $-\chi^2\delta\sigma$ we then see from Eqs. (A25) and (A27) that the quasinormal mode frequency χ for high Λ configurations must go like $1/\Lambda^{0.5}$ for a given $\bar{\sigma}$. We have numerically evolved stars with the same $\bar{\sigma}$ and compared the QNM frequencies obtained to the inverse ratios of the square root of their Λ values for $\Lambda=800$, $\Lambda=1200$ and $\Lambda=1600$, confirming the above analysis. In Table I we show a comparison between the perturbation analysis and the numerical result. We see that the perturbation result gets more accurate for increasing Λ. We note that configurations that have the size of a neutron star would have to have Λ of order 10^{38} with QNM frequency of order $\chi=10^{-19}$.

[1] J. R. Primack, D. Seckel and B. Sadoulet, Annu. Rev. Nucl. Part. Sci. **38**, 751 (1988).
[2] E. Seidel and W-M. Suen, Phys. Rev. Lett. **72**, 2516 (1994).
[3] D. J. Kaup, Phys. Rev. **172**, 1331 (1968); T. D. Lee and Y. Pang, Phys. Rep. **221**, 251 (1992); A. R. Liddle and M. S. Madsen, Int. J. Mod. Phys. D **1**, 101 (1992).
[4] P. Jetzer, Phys. Rep. **220**, 183 (1992).
[5] E. Seidel and W-M. Suen, Phys. Rev. D **42**, 384 (1990).
[6] M. Colpi, S. L. Shapiro and I. Wasserman, Phys. Rev. Lett. **57**, 2485 (1986).
[7] J. D. Breit, S. Gupta and A. Zaks, Phys. Lett. **140B**, 329 (1984).
[8] M. Gleiser, Phys. Rev. D **38**, 2376 (1988); **39**, 1257(E) (1989).
[9] P. Jetzer, Fermilab Report No. Conf-88/88-A (unpublished).
[10] T. D. Lee, Phys. Rev. D **35**, 3637 (1987).
[11] M. Gleiser and R. Watkins, Nucl. Phys. **B319**, 733 (1989).
[12] T. D. Lee and Y. Pang, Nucl. Phys. **B315**, 477 (1989).
[13] R. Ruffini and S. Bonozzola, Phys. Rev. **187**, 1767 (1969).
[14] E. W. Mielke and F. E. Schunck, in Proceedings of the 8th M. Grossmann Meeting, edited by T. Piran (World Scientific, Singapore, in press), gr-qc/9801063.
[15] C. Alcock *et al.*, International Astronomical Union Circ. (USA) No. 6068, 1993.
[16] F. E. Schunck and A. Liddle, Phys. Lett. B **404**, 25 (1997).
[17] J. M. Bardeen and T. Piran, Phys. Rep. **96**, 205 (1983).
[18] C. Bona (private communication).
[19] F. V. Kusmartsev, E. W. Mielke and F. E. Schunck, Phys. Rev. D **43**, 3895 (1991).
[20] In [19] with the aid of catastrophe theory the instability of unstable stars is also discussed. Their conclusion on unstable boson stars is that they disperse or collapse while we also show the presence of migrations. This is due to our perturbations being more general, allowing for changes in mass and particle number, while they keep them strictly constant.